Semi-Active Control of 3D- Vertically Isolated Buildings with Divided Skeleton into Inner and Outer Subsystems with MR- Dampers

Sasan Babaei

Submitted to the
Institute of Graduate Studies and Research
in partial fulfillment of the requirements for the degree of

Master of Science
in
Civil Engineering

Eastern Mediterranean University
September 2022
Gazimağusa, North Cyprus

Approval of the Institute of Graduate Studies and Research

Prof. Dr. Ali Hakan Ulusoy
Director

I certify that this thesis satisfies all the requirements as a thesis for the degree of Master of Science in Civil Engineering.

Prof. Dr. Umut Türker
Chair, Department of Civil Engineering

We certify that we have read this thesis and that in our opinion it is fully adequate in scope and quality as a thesis for the degree of Master of Science in Civil Engineering.

Prof. Dr. Mahmood Hosseini
Supervisor

Examining Committee

1. Prof. Dr. Mahmood Hosseini

2. Assoc. Prof. Dr. Mehmet Cemal Geneş

3. Asst. Prof. Dr. Mohammad Reza Bagherzade Karimi

ABSTRACT

In vertical isolation, the lateral load resisting system is divided into two substructures which are stiff with less system mass and flexible with more system mass. As the system experiences an earthquake, vertical isolation benefits from the prominent difference between the periods of the two sub-systems and the damping mechanisms placed between them across the height. Though effective passive isolation techniques are still susceptible to seismic source characteristics. In this study, the semi-active controlled strategy by using the magnetorheological dampers was investigated in a 3D state in 6, 9, and 12- story buildings, with skeletons divided into two inner and outer sub-systems as stiff and flexible parts. The lumped mass 3D models of the buildings are introduced to MATLAB and subjected to 7 bidirectional ground motions. The analysis results showed that the passive control of viscous dampers is only effective in harnessing the stiff sub-system response to nearly half of the uncontrolled building. However, in the soft sub-system, the inter-story drift on average is 16 percent greater than the uncontrolled building. The semi-active control, however, at the stiff sub-system has a maximum roof displacement, acceleration, and inter-story rotation nearly to 10, 40, and 14 percent of the uncontrolled ones. In addition, the average response for the soft sub-system remained less than half.

Keywords: Vertical isolation, Semi-active control, MR damper, Performance-based design

ÖZ

Dikey izolasyonda, yanal yüke dayanıklı sistem; daha az sistem kütlesi ile sert ve daha fazla sistem kütlesi ile esnek olmak üzere iki alt yapıya ayrılır. Sistem bir depreme maruz kaldığında, iki alt sistemin periyotları arasındaki belirgin farktan ve yükseklik boyunca sistemlerin aralarına yerleştirilen sönüm mekanizmalarından dikey izolasyon yararlanır. Etkili pasif izolasyon teknikleri hala sismik kaynak özelliklerine duyarlıdır. Bu çalışmada, iskeletleri rijit ve esnek olarak iki iç ve dış alt sisteme ayrıldığı 6, 9 ve 12 katlı 3 boyutlu binalarda manyetoreolojik sönümleyiciler kullanılarak yarı aktif kontrollü strateji incelenmiştir. Binaların toplanmış kütleli 3 boyutlu modelleri MATLAB'ta modellenmiş ve çift yönlü 7 yer hareketine tabi tutulmuştur. Analiz sonuçları, viskoz damperlerin pasif kontrolünün, yalnızca kontrolsüz binanın neredeyse yarısına karşı katı alt sistem tepkisinden yararlanmada etkili olduğunu göstermiştir. Ancak, yumuşak alt sistemde, katlar arası göreli kat ötelenme, kontrolsüz binaya göre, ortalama yüzde 16 daha fazla olmaktadır. Bununla birlikte, sert alt sistemdeki yarı aktif kontrol, kontrol edilmeyenlerin yaklaşık yüzde 10, 40 ve 14'ine eşit maksimum çatı yer değiştirmesi, ivmesi ve katlar arası dönmeye sahip olmaktadır. Ek olarak, yumuşak alt sistem için ortalama tepki yarıdan daha az kalmaktadır.

Anahtar Kelimeler: Dikey izolasyon, Yarı aktif kontrol, MR damper, Performansa dayalı tasarım

TABLE OF CONTENTS

LIST OF TABLES

LIST OF FIGURES

LIST OF ABBREVIATIONS

EDP	Engineering Demand Parameters
ER	Electrorheological
LQR	Linear Quadratic Regulator
MR	Magnetorheological
MRE	Magnetorheological Elastomer
MRF	Magnetorheological Fluid
MRP	Magnetorheological Polymers
SAC	Simple Adaptive Controller
THA	Time History Acceleration
THD	Time History Displacement
TMDs	Tuned Mass Dampers
X dir	X direction
Y dir	Y direction

Chapter 1

INTRODUCTION

Seismic risk reduction of buildings, particularly high-rise structures, is increasingly intertwined with control strategies. Structural damage, either by damping the imposed force or shifting the predominant period of the structure, can be prohibited. Tuned mass dampers (TMDs) and seismic isolations shift the structure's natural frequency to lower amounts corresponding to fewer spectral accelerations. This allows buildings with more efficient cross-sections to be built using high-strength and less ductile materials. These methods, however, require lateral flexibility at the isolation layer, which can cause large displacement at the base. To address this issue, a damping mechanism is commonly used at the base; however, this approach could trigger higher modes in severe earthquakes and make the system less responsive to smaller ground motions.

The other procedure to control the base displacement at the base isolation is using hybrid control strategies such as tuned mass dampers and tuned liquid column dampers. Regarding this philosophy of design, mid-story isolation and sub-structure isolation were investigated. This, either used for retrofitting an existing building or designing a new one, can change the upper portion of the structure to TMD with great mass decreasing the base isolation's displacement. One of the design-based approaches to benefit from a period shift is vertical isolation. In vertical isolation, the lateral load resisting system is divided into two substructures, one stiff with less system

mass and the other flexible with more system mass. As the system experiences an earthquake, it benefits from the prominent difference between the periods of the two subsystems and the damping mechanisms placed between them across the height.

In addition to period shift, dissipating the seismic energy by dampers can control the lateral response. Case sensitivity of passive dampers and the need for a severe power supply and the probability of structural instability in active control have prompted an increase in studies on semi-active control, which uses a limited amount of energy to adjust the dynamic characteristics of the system. Semi-active control comprises a range of dampers, including a variable orifice, adjustable tuned liquid, variable stiffness, and controllable fluid dampers. The magnetorheological (MR) damper is robustly grown in structural control and can provide a high level of energy at a lower voltage, has fast control response, simplicity of design, and passive control during a power cut or control algorithm.

Semi-active control of MR dampers, although at conventional structures, even adjacent buildings were studied, still vertical isolation was not investigated using semi-active, especially with MR dampers. In this study, the semi-active control strategies by using the magnetorheological dampers were investigated in a 3D state in 6, 9, and 12- story buildings, with the skeleton divided into two inner and outer subsystems as stiff and flexible parts. The lumped mass 3D models of the buildings are introduced to MATLAB and subjected to 7 bidirectional ground motions. The modified Bouc-Wen model is employed to model the hysteretic behavior of the MR dampers. The passive control of viscous dampers was only effective in harnessing stiff subsystem response. The semi-active control, however, reduces the maximum roof displacement, acceleration, and interstory drift for both sub-structures for all ground motions.

Chapter 2

MR DAMPER

These deformable materials are from the smart material categories. The mechanical property and viscosity of this material are affected by the magnetical field. Considering the crystalline structure of materials, magnetic particles, magnetic liquid, ferrofluid MR Foam, and Elastomer are in this category.

2.1 Magnetic Materials and Electromagnet

Based on the crystal structure and how the electrons are placed in the valence layer, materials, as subjected to the magnetic field, respond differently. According to the response to the magnetic field, materials can be classified into paramagnetic, diamagnetic, ferromagnetic, and non-ferromagnetic. [1, 2]

Ferromagnetic materials have the ability to give up their magnetic properties after the magnetic field is removed; Among them, we can mention iron manganese.

Based on the shape of the hysteresis curve, magnetic materials can be classified as hard, such as iron oxide, and soft, such as a solenoid, which is circulating around an iron core. In the hard model, due to the larger area of the hysteresis curve, it retains the magnetic property caused by the electromagnetic application for a longer time.

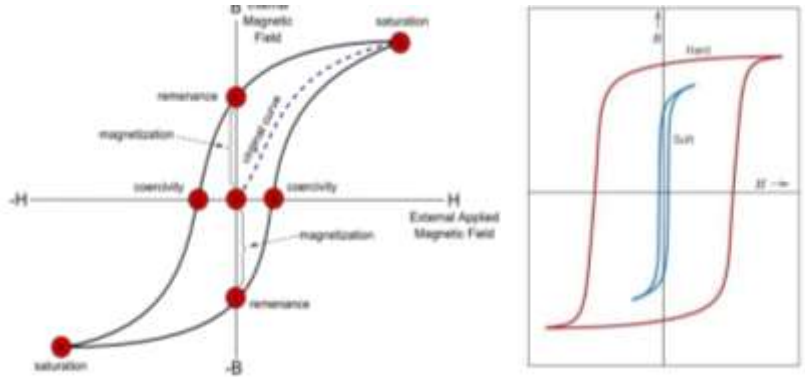

Figure 2.1: a) Hysteresis cycle for a ferromagnetic material; b) Comparing the hysteresis cycle of hard and soft magnetic material [1]

The flow of electric current in a solenoid tube can impose a magnetic field. Faraday's law of electromagnetic induction can be used to describe this phenomenon.

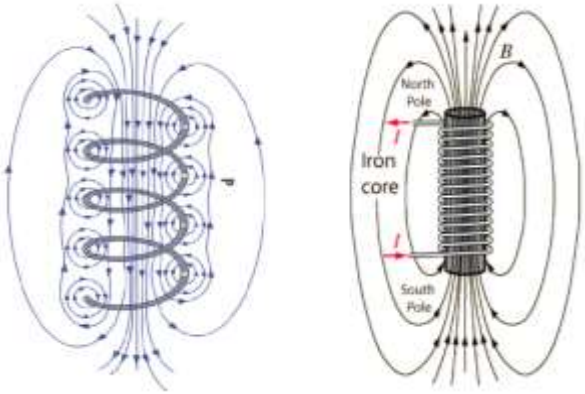

Figure 2.2: Solenoid tube wire [1]

2.2 Fluid Controlled Damper

Materials such as shape memory alloy, piezoelectric, and... due to the crystalline structure by applying stress, temperature, electric or magnetic field change their crystal structure and show different physical properties. Fluid-controlled dampers are a widely used type of this branch; which will be examined in this study.

These dampers include magnetic or electric polarized particles suspended in oil that can be changed from a smooth viscous fluid to a semi-solid material, in which the yield

resistance can be controlled in a few milliseconds or vice versa by increasing or decreasing the intensity of the magnetic or electric field.[3-5]

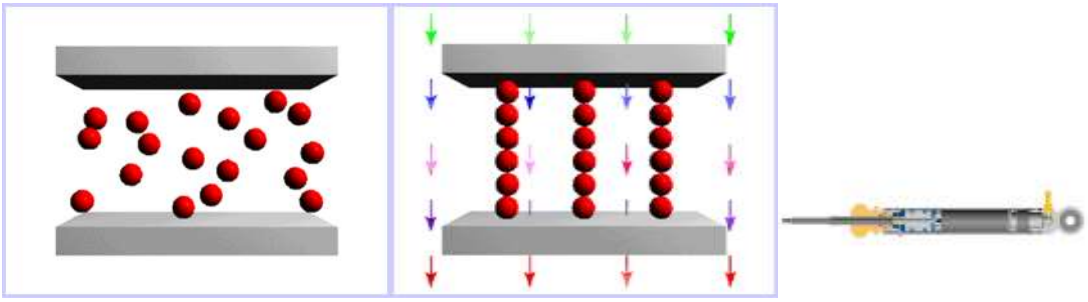

Figure 2.3: MR fluid damper and magnetic field effect [6, 7]

Among the advantages of fluid-controlled dampers is the need for low energy, mechanical simplicity (their only moving component is the piston); Reliable performance, and no need for high maintenance. Fluid-controlled actuators can be referred to as two groups activated by magnetic field MR and electric ER.

2.2.1 ER Fluid-Controlled Damper

These dampers start working under the electric field.

Disadvantages

The inability to achieve high yield stresses, the reduction of the capacity and ability of the ER fluid due to the introduction of impurities such as moisture during construction, the need for maintenance, and a relatively high operating voltage (about 4000 V) is difficult and expensive to provide.[5]

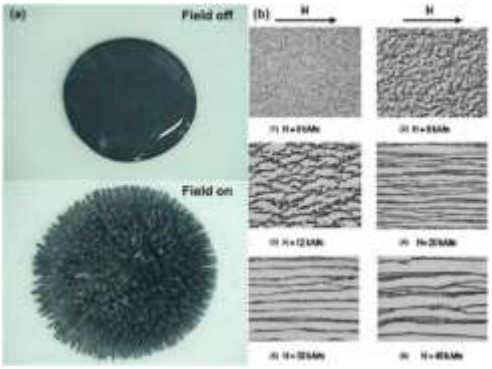

Figure 2.4: Effect of magnetic field [8]

2.2.2 Fluid Controlled Damper (MR)

Viscous liquid, such as Silicon oil, contains magnetically polarized particles, which are polarized by the application of the magnetic current of the liquid and show viscoplastic behavior. The possibility of momentary resistance against the intensity of the magnetic field is one of their other properties.

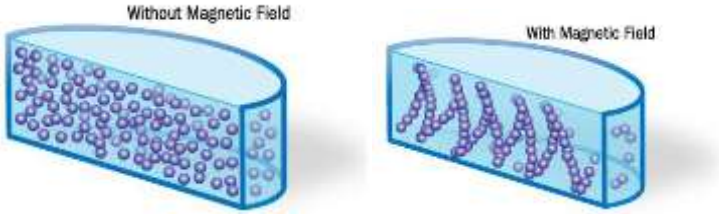

Figure 2.5: Magnetic field effect [3]

2.2.3 Advantages of MR Versus ER Damper

The following advantages can be mentioned for instruments containing these materials:

• High yield stress (about 50 to 100 kPa)

• Impurity does not affect the performance of the damper

• The need for lower voltage around 12 to 24 volts and power less than 50 watts

2.3 MRE Damper

The two most widely used groups are MRF and MRE elastomers. In the first category, they have the ability to change the tension with a high ratio. But the second category shows the ability to change the modulus under the magnetic field. MRP polymers are another group, which has more MR capability than MRE and less precipitation than MRF. These dampers are not suitable for civil engineering due to their low initial modulus.

MREs have the ability to increase their length up to 10%, but the change in characteristics under the magnetic field is the main reason for their use. Among these characteristics, we can mention the change in their stiffness, damping, natural frequency, and viscosity. Unlike the magnetically controlled fluid damper, these dampers do not have problems such as displacement, oil leakage, and environmental pollution. [9-11]

2.3.1 Structure of the MRE

An MRE generally consists of three parts: polarized magnetic components, plastic or elastomer mesh, and additives. Magnetic components can be dispersed homogeneously or form their crystalline structure in gel or elastomer.

Figure 2.6: Structure of the MRE [12]

2.3.2 Polarizable Particles

These separable or magnetic components are dispersed in a non-magnetic or gel-like solid. Among the effective factors in the selection of these components, one can pay attention to the size, geometry and wettability of the components. For example, the size of the components can be from a few micrometers to hundreds of micrometers, which affects the behavior of MRE.

Other factors involved are magnetic permeability, magnetization remnant, and magnetization saturation. Increasing the magnetic permeability increases the effect of MR and decreasing the level of the magnetic field causes the particles to separate after magnetic loading and increases the reverse effect of MR. The most common separable components are spherical iron carbonyls. These components have the effect of magnetic field and high magnetic saturation level and low remnant magnetic level. [12]

2.3.3 Network

The network or host material limits liquid leakage, corrosion problems and accumulation of particles. The network has very little effect on the ability to change MRE, but choosing the right network is very important, especially in long-term use. Natural plastic and silicone plastic are widely used networks.

2.3.4 Additives

Additives are used to modify the behavior mechanism of MRE. Silicone oil, for example, is very popular as an additive. These additives also spread the internal stress in the material. Using black carbon improves the mechanical behavior and reduces the damping coefficient. [13]

2.3.5 Processing of MRE

Based on the manufacturing process, these materials are divided into two parts, isotropic and non-isotropic. In the isotropic model, the behavioral characteristics are similar in all directions. The reason for this is the homogeneity of the distribution of polarizing particles in the entire network. On the other hand, in the heterogeneous model, a chain of particles is formed due to the application of the magnetic field during the construction.

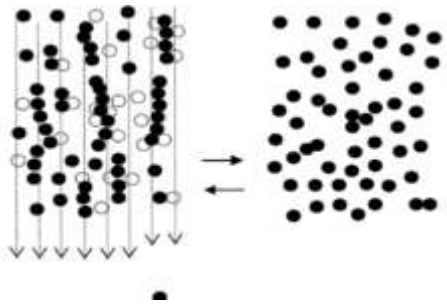

Figure 2.7: Magnetic field during construction [12]

2.3.6 Construction Process

In general, this process includes preparing materials, combining, processing and polymerizing. To process homogeneous materials at room temperature (24°C), the existing air must be evacuated using suction or applying heat. In some cases, a temperature of 120 degrees is also required for processing. During non-isotropic processing, a strong magnetic field of more than 0.8 T is applied. After processing, the particles remain fixed in the network and cannot move freely.

After processing to make stable and durable materials using a chemical process called polymerization, connections between individual polymers are applied in the composition. Improving mechanical behavior and reducing adhesion are other goals of polymerization. MR effect in non-isotropic elastomer is more than isotropic one.

2.4 Mechanical Properties of MRE

These materials behave like materials with viscoelastic properties in the pre-flow regions. In addition to the stiffness, the damping of these materials is also affected by the magnetic field, although it is small. The stress-strain diagram of these materials is therefore directly related to the magnetic field. The figure 2.8 shows the stress-strain diagram for different fields. [12]

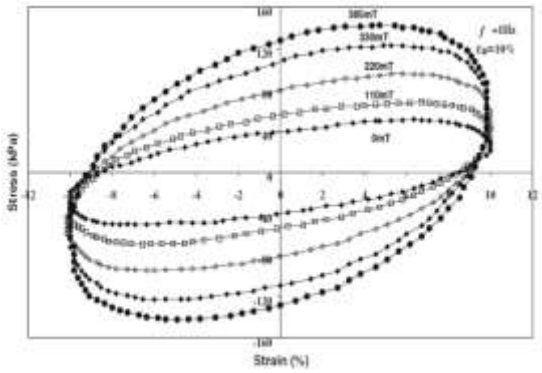

Figure 2.8: MRE stress-strain diagram under different magnetic fields [12]

The most common use of the MRE damper is as a seismic isolator, damper, in the car suspension system and the use of this damper in the sandwich beam. They are used as sensors in micro-electromechanical systems, magnetometers, magnetic resistance, and even as polymers with shape memory.

2.5 Behavioral Modes

Because it is important to know the behavioral modes of the MR damper in modeling it and making an energy-consuming device. The behavior modes of this damper are presented below. [14]

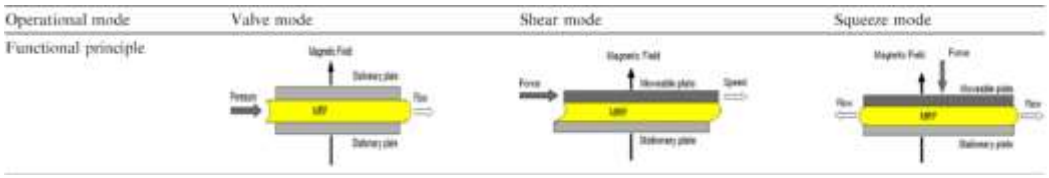

Figure 2.9: Behavioral modes [15]

2.5.1 Pressure Mode

In the pressure mode, the MR liquid is placed in a 0.02-inch-thick plate surrounded by two paramagnetic plates; By changing the distance between two paramagnetic plates, pressure is imposed on the cell. This mode of behavior is suitable for high dynamic loads and low range (mm).

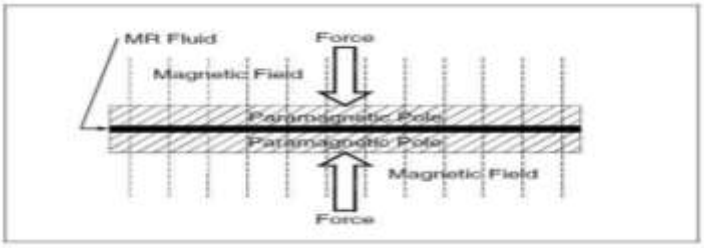

Figure 2.10: Pressure mode for MR [7]

2.5.2 Shear Mode

Unlike the pressing mode, in this mode, cutting is achieved by sliding or rolling two plates on top of each other. The MR fluid this time fits into a 0.015-inch-thick plate. The magnetic field is dependent on the direction of movement of these plates. Examples of the application of this mode include brakes, clutches, dampers, and building composites, which are suitable for relatively small loads.

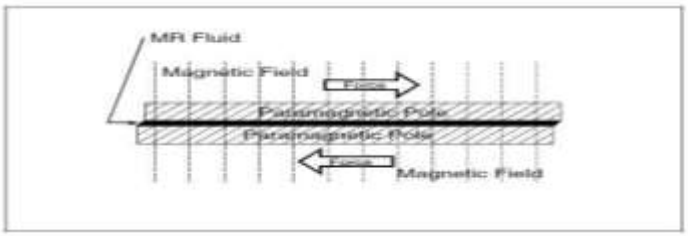

Figure 2.11: Shear mode for MR [7]

2.5.3 Piston Mode

This mode is more widely used than the other two modes. In this mode, there are two tanks of MR fluid that uses a magnetic field to flow from one tank to another; Composed. The current starts by reducing the pressure resistance and is controlled by changing the magnetic current.

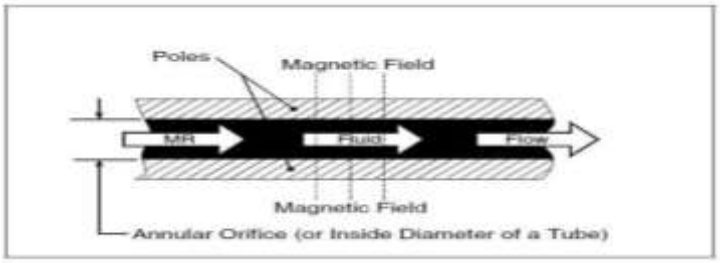

Figure 2.12: Piston mode [7]

2.6 Types of MRF Damper

In general, MRF dampers can be recognized in this grouping based on the type of application and behavioral mechanism. [16]

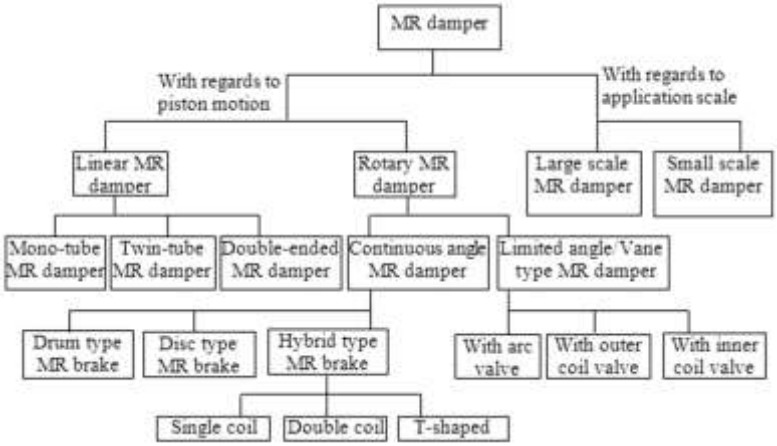

Figure 2.13: MR dampers [16]

The widely used piston dampers, especially in earthquake engineering, are classified into four groups, single tube, pair of tubes, double ends, and hybrid based on the physical structure of the piston.

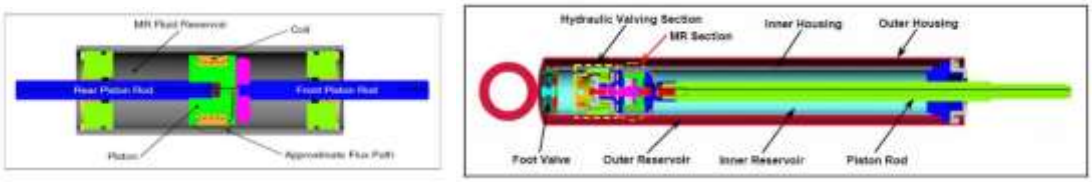

Figure 2.14: a) double end MR damper; b) MR hydraulic hybrid damper [16]

2.7 MR Damper in Buildings

In research by Al- Fahdawi et al., the use of simple adaptive control (SAC), under the effect of noise and changing parameters, was investigated in reducing the response of two coupler structures. One of the advantages of this use is that it is able to respond well to changes in dynamic characteristics such as stiffness and mass. The figure 2.15 shows an n_1 structure and an n_1+n_2 floor structure that are connected using MR. [17]

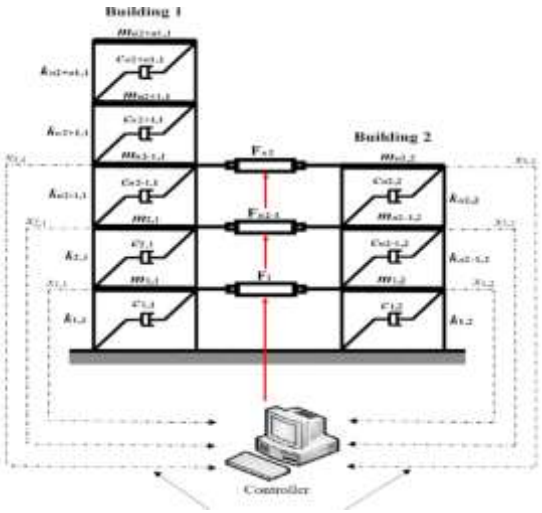

Figure 2.15: Structural model of the control system [17]

Al-Fahdavi et al. investigated the load ponding in two structures of the same height with the MR damper. Two structures of the same height with different dynamic characteristics were coupled together in only 3 floors by the MR damper. SAC and LQR algorithms were also used for control. [18]

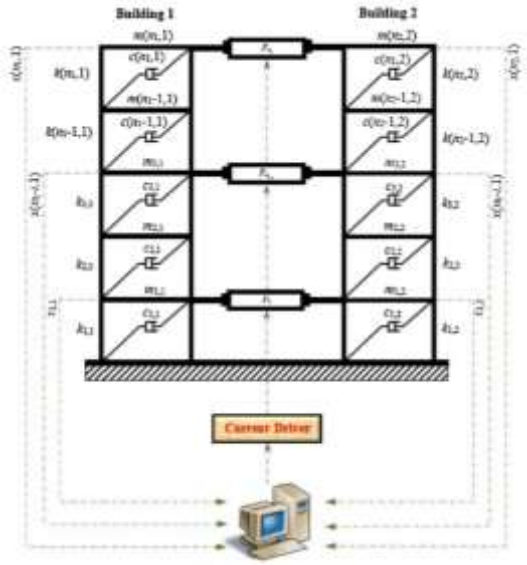

Figure 2.16: Structural 14odelo f the coupled buildings [18]

In research, Yanik and Al-Damir compared and used semi-active MR damper after removing the power supply in the active control system. Because one of the challenges

of active control is the possibility of a sudden interruption of the system; In this research, the combination of active tendon and semi-active MR damper was investigated. Far and near earthquakes, activator voltage and response delay were considered in this research. In this research, the sudden stop has a significant effect on the damping, as well as the delay of the response, did not have a negative effect on the damping. In this model, the active tendon is located in all floors, but the MR damper was placed only in the first floor. [19]

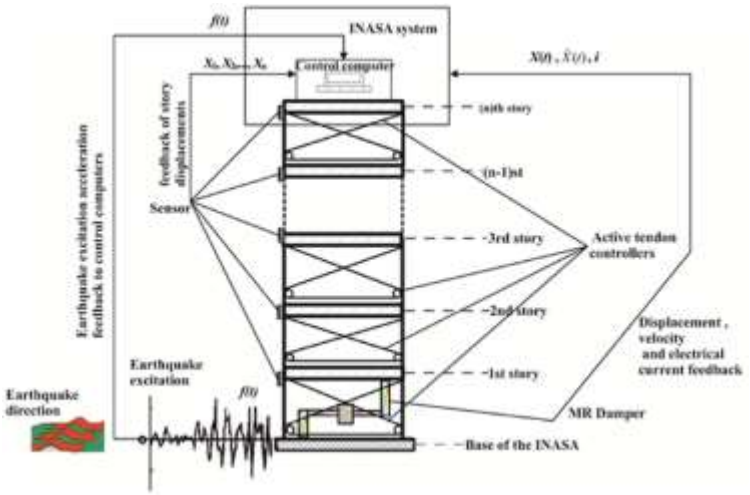

Figure 2.17: INASA control system for n-story structure [19]

2.8 MRE- TMD

Conventional adjustable mass damper shows less usability by changing the dynamic characteristics of the system; Therefore, the use of semi-active systems is one of the solutions for the proper use of this damper. Adjustable mass-magnetic elastomeric damper Although it is a passive damper; It has a better ability than the conventional adjustable mass damper. But in the semi-active mode, adjusting the dynamic characteristics of the system provides a suitable reduction for the response.

The results of Jinchon et al. in the numerical modeling of a 5-story structure showed that the use of this damper using semi-active control greatly reduces the displacement and acceleration responses of the structure.

Figure 2.18: Schematic model of the TMD- MRE [20]

Chapter 3

CONTROL STRATEGIES

Meeting operational and safety limit states can be achieved with structural control methods, which are used to control the vibrations of structural members and the structure itself. In this method, in order to control the structure's response to earthquakes, engineers must somehow limit the energy entering the structure from the ground, or dissipate this energy, or move the frequency of the structure away from the frequency of the seismic load.

Structural controls are generally divided into several groups:

1. Passive control
2. Semi-active control
3. Active control
4. Combined controls

3.1 Passive Control

This system does not use any feedback or energy source to control earthquakes; It depends only on the intrinsic characteristics of the tool, the shape of the tool, and its targeting, which reduces the response of the structure by wasting energy or changing the dynamic characteristics of the structure.

The randomness of the seismic loads applied to the structure and the constancy of the inherent characteristics of the passive control tool such as mass, stiffness, and damping

cause; these tools are affected by the seismic load frequency compared to the initial assumption. But since these tools do not need external energy, they are a low-cost approach. Shear wall braces, bending frame, base isolation system friction joints, viscoelastic damper, viscous liquid damper, adjusted mass damper, and flowing metal dampers... are among many passive control methods of the structure.

3.1.1 Advantages

- No need for an external source
- Lack of instability caused by external force
- Low maintenance cost

3.1.2 Disadvantages

Application limitation for specific stimuli due to having fixed dynamic characteristics (mass, hardness, cycle time, and damping).

3.2 Semi-Active Control and Its Advantages

In this type of system, control tools with a small force have the ability to change their characteristics such as stiffness and damping in relation to the applied load or its history.Semi-active adjusted mass damper, adjustable liquid column damper, and variable input damper... can also be considered semi-active control methods. The purpose of this control is to protect the structure with limited energy:

• Better performance than passive control

• Moment-to-moment adaptation (active control) with limited energy

• Lack of instability caused by an external force

• High reliability as a passive system

• Possibility of passive behavior in case of power supply damage

3.3 Types of Semi-Active Control Systems

1. Damper with variable valve

2. Damper with variable hardness

3. Damper with balanced semi-active mass

4. Damper with controlled liquid column

5. Damper with controlled fluid

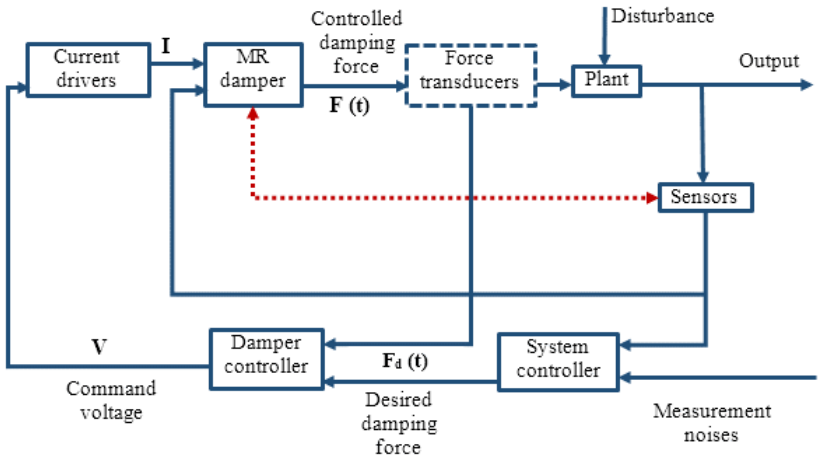

Figure 3.1 Application diagram of MR damper control in semi-active control [16]

3.4 Active Control

These systems consist of three parts: measuring system, computer monitoring system and control mechanism. This mechanism has the task of applying force to the structure during the passage of displacement and acceleration of a certain limit. Depending on the external stimuli and changes in the structure's response, they are divided into two parts, open circuit or closed circuit.

These include active stiffness damper, active mass system, active bracing system and active cable control system. The purpose of this control is to protect the structure

during an earthquake or wind. In this process behavior of the building by applying an external force against the direction of the seismic force is controlled.

3.4.1 Advantages

Compliance with incoming load

3.4.2 Disadvantages

The need for complex systems and intelligent control to apply force and appropriate algorithms to determine the optimal force is the limitation of this method. The need for a lot of external energy can lead to the instability of the structure.

3.5 Hybrid Controls

Active control, which mainly requires heavy computer processing and must be used continuously, can be combined with a semi-active control; This control is called hybrid control. Such hybrid methods have the advantage, that when the computer processing is suddenly out of reach, other systems perform their control capability.

3.6 Mass Isolation

Seismic isolation shifts a structure's natural frequency to lower amounts corresponding to less spectral accelerations. This allows buildings with more efficient cross-sections to be built using high-strength and less ductile materials. Although elimination of higher-mode effects will cause the building behavior to be mostly linear and more predictable in seismic events, the need for lateral flexibility at the isolation layer can cause large displacement at the base.[21] However, designing large gaps is economically infeasible in urban environments. To address this issue, a damping mechanism is commonly used at the base; however, this approach could trigger higher modes in severe earthquakes and make the system less responsive to smaller ground motions. [22] Base displacement also can be controlled using hybrid control strategies such as tuned mass dampers and tuned liquid column dampers. [23-25]

The need to reduce base displacement is a facet of structural design. Mid-story and multi-layer isolation can reduce base displacement by transmitting it to the upper stories. This is efficient primarily for tall buildings surrounded by lower structures. One practical use of mid-story isolation is in the retrofitting of the existing buildings. When excavating for a base isolation system, temporary support works are normally required. Mid-story isolation can reduce the disruption of occupancy and the project cost. It also can allow for an extra floor to be constructed on an existing building.

Mid-story isolation converts the upper structure to a tuned mass damper having a large mass that is designed to control the lower portion of the structure. [26] Skandalos et al. used meta-heuristic optimization and multiple layers of isolation to reduce the seismic response of a building. Their study also suggested that isolation layers should be installed at the lower portion of a building. [27]

Ma et al. numerically analyzed conventional and base isolation systems with adding stories. They compared the response of structures under far- and near-field pulse-like records and found that base isolation, by elongating the period, can effectively reduce the seismic demand. [28] Becker and Ezazi reported that double-layer isolation decreased the relative displacement of the first story by 48%. This procedure also increased upper-story displacement by 19%. [29] Kim and Kang used semi-active control by a MR damper and mid-story isolation in tall buildings to decrease the isolation layer and the inter-story drift with multi-objective optimization. [30]

Partial mass or vertical isolation can be used to address base isolation and TMD drawbacks, especially when isolation of the whole structure is not efficiently feasible. In their method, only one portion of the structure was isolated. An upper-story mega-

sub isolation system and floor isolation are examples of this approach. In this process, the mass of the structural elements is used as the tuning effect. [31] Anajafi and Medina analyzed 6-, 12- and 20-story buildings under Kanai-Tajimi filtered Gaussian white noise excitation. The results indicated that the response reduction was similar to a tuned mass damper and base isolation, decreasing the traditional deficiency of the base isolation, without imposing any mass on the system. [32]

Similar to coupled structure, vertical isolation takes the mass of the structure under consideration for isolation purposes, which reduces the design complexity at the base. [33] In such a system, the structure should be divided into two substructures, one stiff with less system mass and the other ductile with more system mass. [34, 35] As the system experiences an earthquake, it shows a prominent period shift, but benefits from damping mechanisms placed between the two substructures across the height. Milanchian and Hosseini used non-linear, rather than linear viscous dampers for vertical isolation and reported no significant difference in response reduction. Nonetheless, the suitable ratio for mass and stiffness could reduce the substructural drift. [36]

Chapter 4

BEHAVIORAL MODELS AND CONTROL ALGORITHM

4.1 Behavioral Models

Parametric and non-parametric methods are used to model MR damper behavior. The behavior of the nonlinear damper and hysteresis is obtained in the parametric model by assimilating the behavior of the experimental structure and the arrangement of springs and dampers. [6]

4.1.1 Bingham Plastic Model

One of the most common models for modeling the behavior of the MR damper is. Behavior is rigid; As long as the stress exceeds the minimum yield stress, the behavior of the material is linear. This model was first used for ER and then for MR. This model is not able to describe the behavior of the damper when the signs of acceleration and velocity are opposite and the magnitude of the velocity is low; to model It also does not cover the hysteresis behavior well. [37]

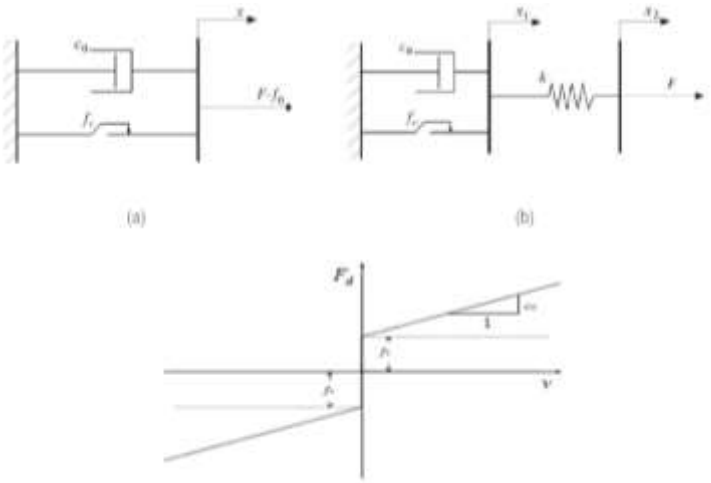

Figure 4.1: Bingham plastic model [6]

4.1.2 Gamata and Flisko Models

One of the modifications to the Bingham model, which was first developed for ER dampers and then for MR dampers, although it captures the force-displacement and force-velocity relationship well; But due to the prevailing difficulty, its numerical modeling becomes very difficult. [38]

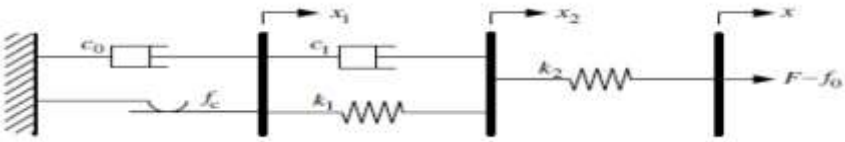

Figure 4.2: Gamata and Flisko models [3]

4.1.3 Bouc-Wen Model

This model is very adaptable and able to model hysteresis behavior. In this model, when the signs of acceleration and speed are opposite and the size of the speed is low, it does not match with reality. [39]

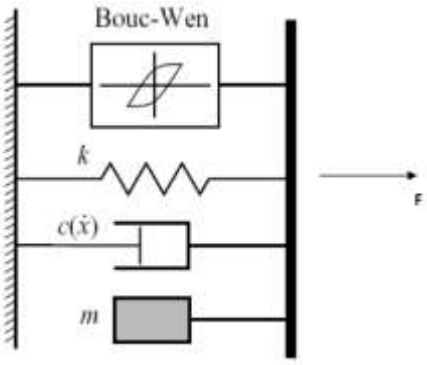

Figure 4.3: Bouc-Wen model [39]

4.1.4 Modified Bouc-Wen Model

The Bouc-Wen model initially was used by Spencer et al. to predict the behavior of an MR damper. It then was modified by Spencer to accommodate nonlinearity more accurately[40]. The model depicted in Fig. 4.4 accommodates an extra dashpot and a spring to compensate for defects in model prediction at low velocities and the effect of the gas chamber. [1]

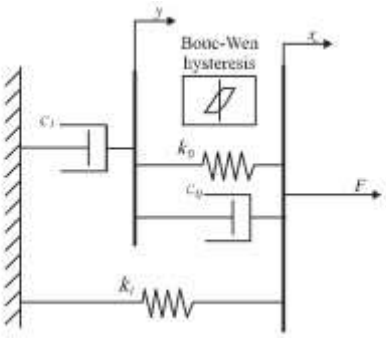

Figure 4.4: Modified Bouc-Wen model for MR damper. [41]

The damping force of the MR damper is given by[40]:

$$f_{mr}^{i} = C_1\dot{y}_1 + K_1(X_{i+n} - X_i - X_0) \quad (1)$$

Where y_i is the internal pseudo-displacement and z_{di} is the evolutionary variable.

$$\dot{y}_1 = \frac{1}{(C_0 + C_1)}\{\alpha z_{di} + C_0(\dot{x}_{n+i} - \dot{x}_i) + K_0(X_{n+i} - X_i - y_i)\} \quad (2)$$

$$\dot{z}_{di} = -\gamma|\dot{x}_{n+i} - \dot{x}_i - \dot{\gamma}_i|z_{di}|z_{di}|^{n_a-1} - \beta(\dot{x}_{n+i} - \dot{x}_i - \dot{\gamma}_i)|z_{di}|^{nd} + A_c(\dot{x}_{n+i} - \dot{x}_i - \dot{y}_1) \quad (3)$$

Where x_i is the displacement of the i^{th} floor, K_0 and k_1 are the accumulator stiffness and the stiffness at large velocities, respectively, and x_0 is the initial displacement of spring k_1. The viscous damping observed at higher and lower velocities are denoted by c_0 and c_1, respectively, and α is an evolutionary coefficient.

$$\alpha = \alpha_a + \alpha_b u;\ C_1 = C_{1a} + C_{1b}u;\ \ C_0 = C_{0a} + C_{0b}u \quad (4)$$

Where u is the output of the following first-order filter:

$$\dot{u} = -\eta(u - v_i) \quad (5)$$

and v_i is the command input voltage of the damper on the i^{th} floor. The parameters of the Bouc-Wen phenomenological model for the 1000 kN MR damper are presented in table 4.1.

Table 4.1: Parameters of Bouc-Wen phenomenological model for 1000 kN MR dampers. [42]

Parameter	Value	Parameter	Value
c_{0a}	50.30 kN sec/m	α_a	8.70 kN/m
c_{0b}	48.70 kN sec/m/V	α_b	6.40 kN/m/V
k_0	0.0054 kN/m	γ	496.0 m^{-2}
c_{1a}	8106.2 kN sec/m	β	496.0 m^{-2}
c_{1b}	7807.9 kN sec/m/V	A_c	810.50
k_1	0.0087 kN/m	n_d	2
x_0	0.18 m	η	195 sec^{-1}

4.2 Control Algorithm

4.2.1 Linear Quadratic Regulator

A linear quadratic regulator (LQR) is a classic, simple and well-known method of optimal control. The control vector should be calculated to minimize the quadratic cost function as: [43]

$$J_{lqr} = \int_0^{\infty} \{x_P(t)^T Q_{lqr} x_P(t) + u_P^T(t) R_{lqr} u_P(t)\} dt \tag{6}$$

The magnitude of decrease in the state variables and the control forces are balanced by weighting matrices Q_{lqr} and R_{lqr}. The values selected to tune the results were:

$$Q_{lqr} = \frac{1}{2}\begin{bmatrix} K & 0 \\ 0 & M \end{bmatrix} \tag{7}$$

$$R_{lqr} = \rho I_{(n1+2n2, n1+2n2)};\ \rho = 1 \times 10^{-7.2} \tag{8}$$

4.2.2 Fuzzy Logic Algorithm

Unlike conventional zero and one logic, in fuzzy logic variables can be continuous. In the input stage, the sensor data is defined using equations (triangular, trapezoidal, bell-shape function) and the calculation process is performed using a series of what-ifs. Zhou et al. used MR damper and fuzzy logic to control a single and multi-level structure. In multi-objective optimization, Elavahat and Ramsavari used genetic algorithm and fuzzy logic to control a benchmark structure under earthquake and wind load. Kim et al proposed a multi-input and multi-output fuzzy logic for small-scale structural models; which was finally investigated in an eight-story structure equipped with an MR damper.

4.2.3 Simple Adaptive Controller

In this method, the response is optimized by forcing the controlled structure to behave like the reference model with the desired trajectories. The control force is determined by the feedback error between the plant and the reference model. Computation of the

adaptive gains does not require explicit system identification or observation. The linear equation governing the reference model and the plant are: [41]

$$\dot{x}_P(t) = A_P x_P(t) + B_P u_P(t) + d_i(t) \quad (9)$$

$$y_P(t) = C_P x_P(t) + D_P u_P(t) + d_o(t) \quad (10)$$

$$\dot{x}_m(t) = A_m x_m(t) + B_m u_m(t) \quad (11)$$

$$y_m(t) = C_m x_m(t) + D_m u(t) \quad (12)$$

The error and the control command are:

$$e_y(t) = y_m(t) - y_P(t) \quad (13)$$

$$u_P(t) = K(t) r(t) \quad (14)$$

Where r(t) is the reference vector and is equal to:

$$r^T(t) = \left[\left(y_m(t) - y_P(t) \right)^T x_m^T(t) u_m^T(t) \right] \quad (15)$$

K(t) is the gain matrix made up of the integral and proportional gains, which are: [41, 44]

$$K(t) = K_I(t) + K_P(t) \quad (16)$$

$$\dot{K}_I(t) = e_y(t) r(t)^T T - \sigma K_I(t) \quad (17)$$

$$K_P(t) = e_y(t) r(t)^T T \quad (18)$$

In which T and T^{-} are tuning matrices which should be optimized by the operator to modify the adaptation rate. The σ-term contains small values and is used to prevent divergence in the results of the equation. Figure 4.6 shows a block diagram representing the adaptive control system.

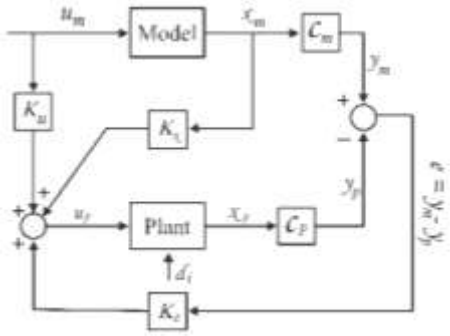

Figure 4.5: Block diagram of simple adaptive controller. [8]

4.2.4 Lyapunov Stability Theory-based Algorithm

Lyapunov theory of stability is a direct control strategy in a feedback controller design. A positive definite Lyapunov function of the states of the system should be used to control the stability of the system. One function previously used by Leitmann is: [45]

$$L(y) = \frac{1}{2}\|x_P(t)\|_P \tag{19}$$

Where the P-norm of the system state is equal to:

$$\|x_P(t)\|_P = [x_P(t)^T P_L x_P]^{1/2} \tag{20}$$

P_L in Eq. (21) is a real, symmetric, positive definite matrix governed by the following equation:

$$A_P^T P_L + P_L A_P + Q_L = 0 \tag{21}$$

In which Q_L is a positive definite matrix that can be selected.

The derivative of the Lyapunov function of the solution of state-space and the control law which will minimize it are:

$$\dot{L}\big(y(t)\big) = -\frac{1}{2}x_P(t)^T Q_L x_P(t) + x_P(t)^T P_L B f_m(t) + x_P(t)^T P_L E\ddot{x}_g(t) \tag{22}$$

$$v_i = V_{max} H\big(-x_P(t)^T P_L B\, f_m(t)\big) \tag{23}$$

Where H(.) is the Heaviside function. This equation establishes that the control voltage is either V_{max} or zero.

4.3 Measurement

The uncontrolled, passively controlled and semi-actively controlled structures were analyzed under 7 bidirectional seismic records taken from the PEER Ground Motion Database in line with FEMA P-695. [46] Roof displacement, interstory drift, and floor acceleration were the performance measures used. These performance criteria are evaluated as: [47]

$$J_1 = \frac{\max(|x_i(t)|)}{x_{unctrl}} \tag{24}$$

$$J_2 = \frac{\max(|d_i(t)|)}{d_{unctrl}} \tag{25}$$

$$J_3 = \frac{\max(|\ddot{x}_i(t)|)}{\ddot{x}_{unctrl}} \tag{26}$$

Where J_1, J_2, and J_3 are the displacement, acceleration, and drift criteria that establish the efficiency of the control strategies. Hazus recommendations were used to evaluate the structural performance as presented in table 4.2.

Table 4.2: Structural performance levels for reinforced concrete moment-resisting frames. [48]

Interstory drift at threshold of damage state			
Slight	Moderate	Extensive	Complete
0.0025	0.005	0.015	0.04

Chapter 5

MODEL AND NUMERICAL EXAMPLES

5.1 One Story Modeling

In order to portray the dynamic characteristics of the system, lumped mass model at the 3D state was used. In this model, masses are concentrated at sub- systems floor and each floor of the inner and outer sub- system was joined with two translational stiffness and damping at X and Y direction, and one torsional stiffness and damping. The one story as depicted in the figure 5.1 contains 6 degrees of freedom.

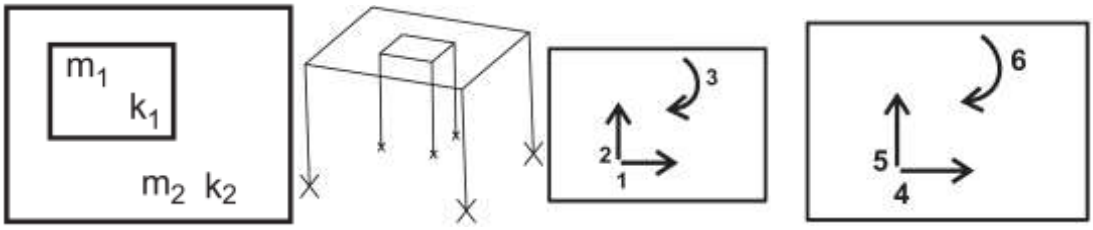

Figure 5.1: Schematic model of one- story building

The matrix equation of the structural system motion can be written as:

$$[M_s]\{\ddot{x}(t)\} + [C_s]\{\dot{x}(t)\} + [K_s]\{x(t)\} = [J]\{f_m(t)\} - [M_s][\Lambda]\ddot{x}_g(t) \quad (27)$$

Where M, K, and C are the mass, stiffness and damping matrices of the coupled system, f_m is the MR damper force vector, and J is the matrix that defines the location of the control forces. The mass and stiffness matrices can be expressed as:

$$m = \begin{bmatrix} m_1 & 0 & 0 & 0 & 0 \\ 0 & m_1 & 0 & 0 & 0 \\ 0 & 0 & m_1 \dfrac{(b_1^2 + d_1^2)}{12} & 0 & 0 \\ 0 & 0 & 0 & m_2 & 0 \\ 0 & 0 & 0 & 0 & m_2 \dfrac{(b_2^2 + d_2^2)}{12} \end{bmatrix} \quad (28)$$

$$k = \begin{bmatrix} k_1 + kd_x & 0 & 0 & -kd_x & 0 & 0 \\ 0 & k_2 + kd_y & 0 & 0 & -kd_y & 0 \\ 0 & 0 & k_3 + kd_\theta & 0 & 0 & -kd_\theta \\ -kd_x & 0 & 0 & k_4 + kd_x & 0 & 0 \\ 0 & -kd_y & 0 & 0 & k_5 + kd_y & 0 \\ 0 & 0 & -kd_\theta & 0 & 0 & k_6 + kd_\theta \end{bmatrix} \quad (29)$$

Where m_1, m_2, b_1, b_2, d_1, and d_2 are the mass, length, and width of each unconnected sub- systems. K_1, k_2, k_3 are the translational and rotational stiffness of the stiff sub-structure and k_4, k_5, and k_6 are theses stiffness for the soft sub- system. K_x, k_y, and k_θ are the translational and rotational stiffness of the dampers.

5.2 n- Story Building

The n- story building by considering the same procedure used to model the one-story building is modeled. Each sub-system, therefore, has 3n degrees of freedom n DoFs in X and n DoFs in the Y direction and n rotational DoFs. The whole structure has 6n DoFs.

Schematic figure of the structure and DoFs of the system at the i^{th} floor is presented in the figure 5.2.

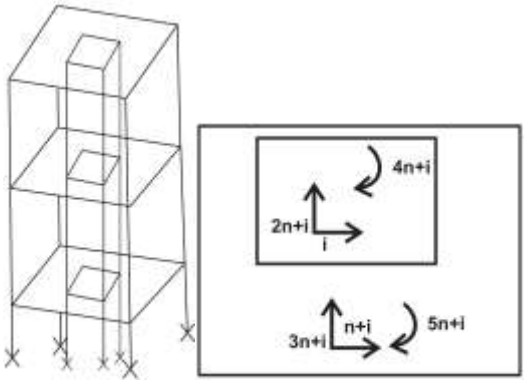

Figure 5.2: a) Schematic model of n- story building; b) DoF at ith floor

The 6n DoFs mass matrices of the system can be shown as:

$$m = \begin{bmatrix} m_1 I_n & & & & & \\ & m_2 I_n & & & & \\ & & m_1 I_n & & & \\ & & & m_2 I_n & & \\ & & & & I_{\theta_1} & \\ & & & & & I_{\theta_2} \end{bmatrix} \quad (30)$$

Where m_1, and m_2 are the floor masses of the inner and outer sub-systems. In is an eye matrix. I_n can be calculated by the following formula.

$$I_{\theta_1} = I_n . m_1 \frac{(b_1^2 + d_1^2)}{12} \quad (31)$$

$$I_{\theta_2} = I_n . m_1 \frac{(b_2^2 + d_2^2)}{12} \quad (32)$$

The stiffness matrix of the MDOF system can be expressed as:

$$k_{(6n,6n)} = \begin{bmatrix} k_{I_{x1}} & & & & & \\ & k_{I_{x2}} & & & & \\ & & k_{I_{y1}} & & & \\ & & & k_{I_{y2}} & & \\ & & & & k_{I_{\theta 1}} k_{I_{\theta 2}} & \end{bmatrix} \quad (33)$$

$$+ \begin{bmatrix} \begin{bmatrix} kd_x & -kd_x \\ -kd_x & kd_x \end{bmatrix} & & & \\ & \begin{bmatrix} kd_y & -kd_y \\ -kd_y & kd_y \end{bmatrix} & & \\ & & \begin{bmatrix} kd_\theta & -kd_\theta \\ -kd_\theta & kd_\theta \end{bmatrix} & \end{bmatrix}$$

This matrix is composed of two matrices. The first is the diagonal stiffness matrix of the substructure and the second is the effect of the damper placed between the two sub-systems. In this equation, k_1 and k_2 are the results of the mass, frequency ratio, the number of stories in the substructures, and the stiffness of the non-isolated building. They can be obtained by coding in MATLAB. I_x is the stiffness matrix of an n-story frame with a stiffness equal to one.

k_θ is the torsional stiffness of the system. As can be seen in the figure 5.3, 0.5 of the system stiffness for x and y directions is concentrated at the floor's center and 0.25 of the stiffness is concentrated on the other sides.

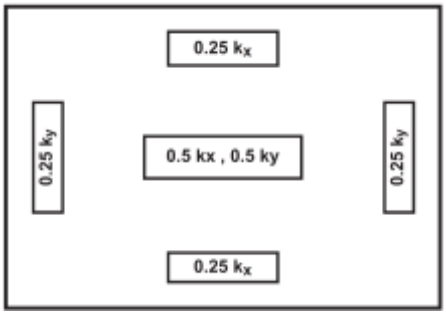

Figure 5.3: Stiffness distribution of the floors

Torsional stiffness of the sub-system by assuming equal length for floors can be evaluated by the following formulas.

$$kI_{x_1} = \begin{bmatrix} K_1 + k_2 & -k_2 & & \\ -k_2 & K_2 + k_3 & & \\ & & & k_{n-1} - k_n \\ & & -k_n & k_n \end{bmatrix} \quad (34)$$

$$k_\theta = 2\left(\frac{1}{4}k_x\frac{d^2}{4} + \frac{1}{4}k_y\frac{b^2}{4}\right) \quad (35)$$

$$k_\theta = k_x\frac{d^2}{4} \quad (36)$$

The kd_x is the damping matrix of the dampers and can be expressed as:

$$kd_x = \begin{bmatrix} Kd_1 & & & \\ & Kd_2 & & \\ & & kd_i & \\ & & & kd_n \end{bmatrix} \quad (37)$$

Kd_i is the stiffness of the damper at the i^{th} story of the system.

For the passive control, the viscous damping criteria introduced at the FEMA 356 is used to calculate the damping effect between two substructures (American Society of Civil Engineers 2000). The damping matrix of C_d can be calculated as:

$$C_d = \begin{bmatrix} C_{c1} & 0 \\ 0 & C_{c2} \end{bmatrix} \quad (38)$$

The damping coefficients between floors is assumed to be equal and are expressed as:

$$\beta_{1,2} = \frac{\left(\max\{T_{s_1,1}, T_{s_2,1}\}\right)\sum_j c_{cj}(\emptyset_{j,1} - \emptyset_{j,2})^2}{4\pi\sum_i m_i\emptyset_i^2} \quad (39)$$

5.3 Numerical Example

In this study, multi- story building with 6,9, and 12 stories with the predominant period of 0.6991, 0.9476, and 1.1758 respectively was modeled in MATLAB. The lumped mass model with the mass placed at the center of the floors was used to model the building. Adjacent floors of the sub-structures were connected by the dampers. Each sub-structure contains 3n degrees of freedom at X and, Y direction, and rotational displacement. The whole structure, therefore, contains 6n degrees of freedom. The floors are rigidly connected by dampers. Any effect of soil on the structure was neglected and the plans of the structures were considered to be symmetric.

In order to reduce the analysis time, the state-space was used. Due to sequential environment of the semi- active control, the MATLAB software was used to calculate the control force and displacement at each step.

Chapter 6

RESULT AND DISCUSSION

In this chapter, the time history response of the three 6 9, and 12-story structures were analyzed. The roof displacement, acceleration, and interstory rotation of each building acquiring passive and semi-active control compared with an uncontrolled alternative.

6.1 Six-Story Building

The time history analysis of the six-story building delineates that passive mass isolation can reduce the engineering demand parameters (EDP) namely, roof displacement and acceleration by 2 3 times regarding the record applied to the structures. On the other hand, the semi- actively controlled structure can contain by 10 times reduction in its EDP. The graphs easily reveal the acceleration reduction which increases the resident's comfort rather than safety during lateral load is not as much as the displacement reduction.

6.1.1 Time History of Roof Displacement

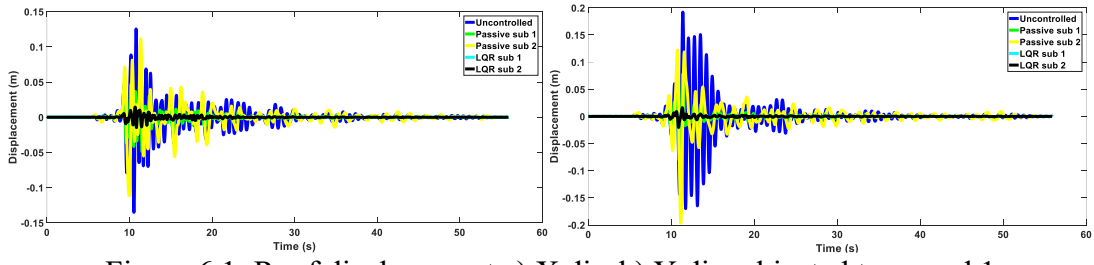

Figure 6.1: Roof displacement a) X dir; b) Y dir subjected to record 1

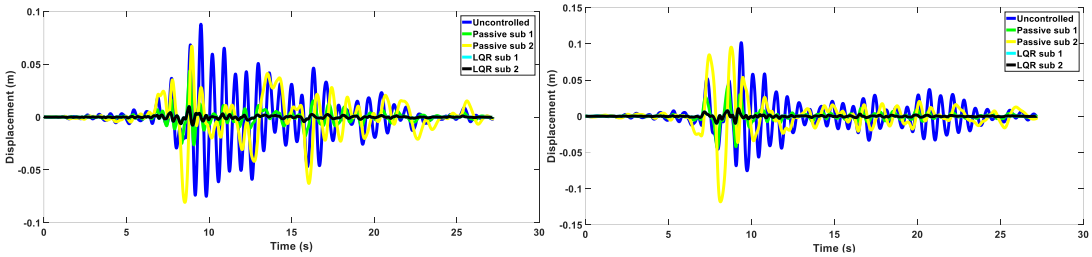

Figure 6.2: Roof displacement a) X dir; b) Y dir subjected to record 2

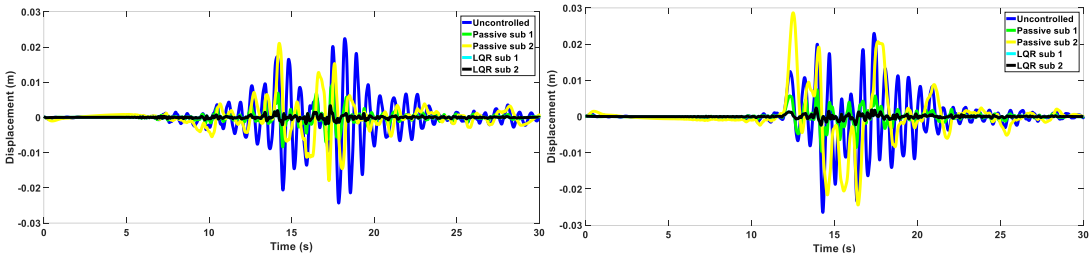

Figure 6.3: Roof displacement a) X dir; b) Y dir subjected to record 3

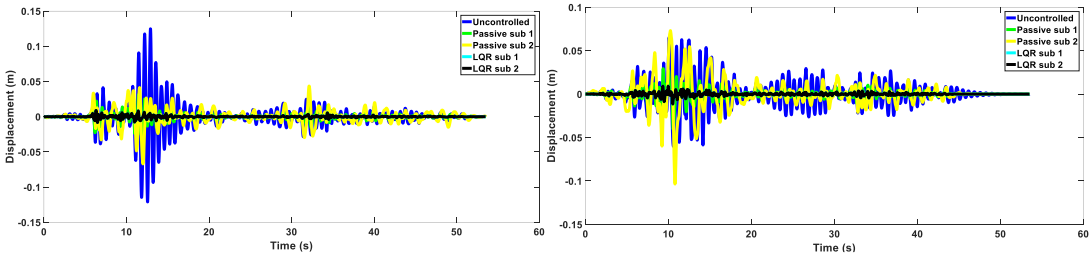

Figure 6.4: Roof displacement a) X dir; b) Y dir subjected to record 4

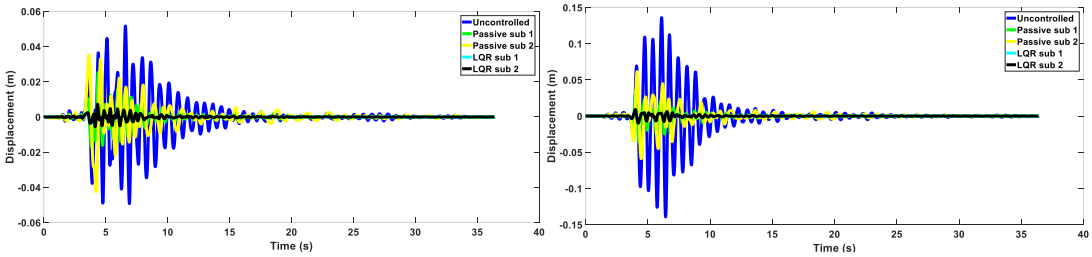

Figure 6.5: Roof displacement a) X dir; b) Y dir subjected to record 5

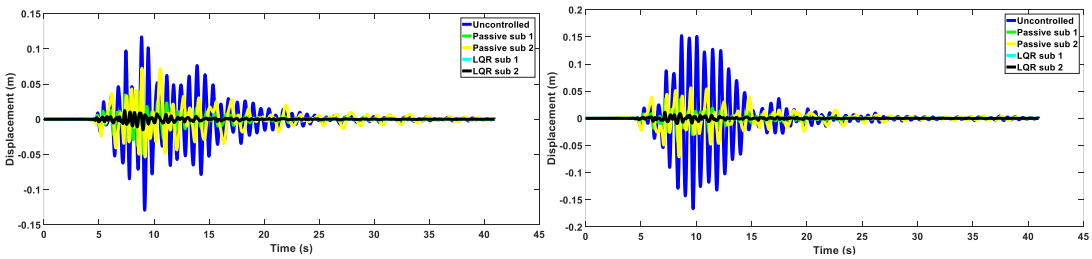

Figure 6.6: Roof displacement a) X dir; b) Y dir subjected to record 6

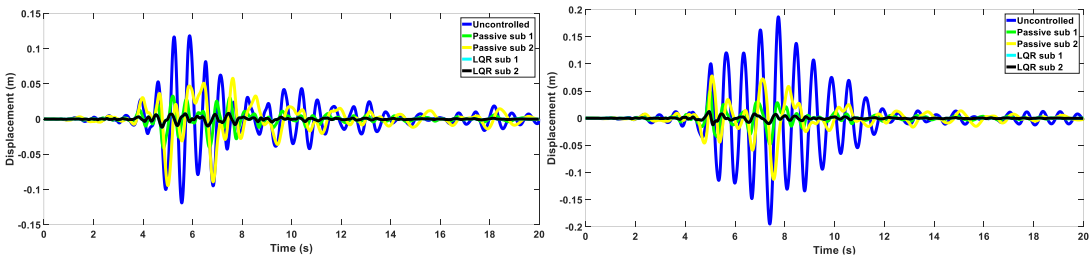

Figure 6.7: Roof displacement a) X dir; b) Y dir subjected to record 7

As has been provided in table 6.1 in the X direction the passive stiff sub- and soft sub-structures have 0.3705, and 0.7284 of the average roof displacement of the uncontrolled structure respectively. These numbers for the average of 7 records for roof displacements are 0.1056 and 0.2752. These reductions for Y direction for the average of the 7 records are 0.3422, and 0.7803 for the passive controlled. In the semi-active control case, the roof displacement of the two sub-structures are 0.0970, and 0.2949 of the uncontrolled structure.

Table 6.1: Max roof displacement X- dir

Record	Uncontrolled	Passive Sub 1	Passive Sub 2	LQR Sub 1	LQR Sub 2
1	0.1351	0.0489	0.1115	0.0147	0.0439
2	0.0880	0.0438	0.0807	0.0100	0.0278
3	0.0243	0.0094	0.0210	0.0034	0.0088
4	0.1249	0.0316	0.0671	0.0090	0.0244
5	0.0517	0.0254	0.0426	0.0073	0.0160
6	0.1293	0.0492	0.0724	0.0151	0.0315
7	0.1190	0.0408	0.0944	0.0115	0.0326

Table 6.2: Max roof displacement Y- dir

Record	Uncontrolled	Passive Sub 1	Passive Sub 2	LQR Sub 1	LQR Sub 2

1	0.1922	0.0814	0.1964	0.0203	0.0622
2	0.1017	0.0437	0.1181	0.0105	0.0356
3	0.0265	0.0096	0.0287	0.0024	0.0112
4	0.0652	0.0406	0.1035	0.0114	0.0297
5	0.1394	0.0366	0.0615	0.0098	0.0249
6	0.1666	0.0422	0.0709	0.0113	0.0622
7	0.1949	0.0493	0.1126	0.0203	0.0356

The bar chart in figure 6.8 easily portrays that using control, especially semi-active control reduces both inner and outer sub- systems displacements. The soft- subsystem as inherent a long period gain more displacement for both controls, which are still less than the uncontrolled response.

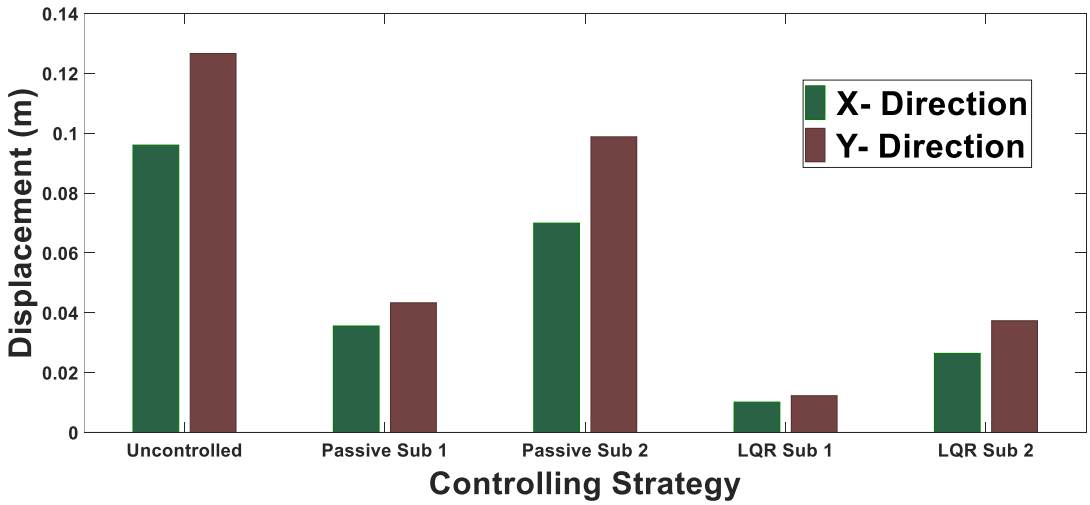

Figure 6.8: Average max displacement regarding control and directions

6.1.2 Time History Acceleration

The graphs depict that utilizing a control strategy, especially semi-active control decreases the roof acceleration when subjected to the ground motion. This reduction

plays a substantial role to increase the comforts of the owners. The table also reveals, unlike displacement the stiff and soft sub-structures experience the quite same reduction in their average maximum response for their maximum acceleration at the roof. The ratios of the max average accretion for soft, and stiff sub- structures subjected to the 7 bidirectional records for the passive control are 0.6456, and 0.5531 respectively. This ratios for the semi- actively controlled structure are 0.4057, and 0.3794 respectively.

This number for the Y direction reduced more than the X direction which are equal to 0.5739, and 0.5426 for the passive sub-structures. For the semi- actively controlled structure the ratio are 0.3318, and 0.2334 respectively.

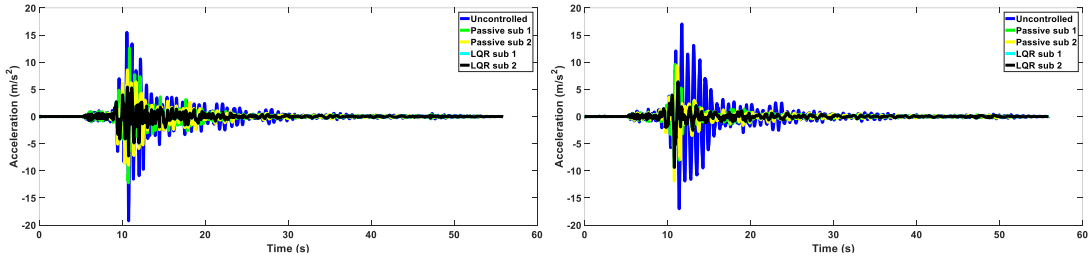

Figure 6.9: Roof acceleration a) X dir; b) Y dir subjected to record 1

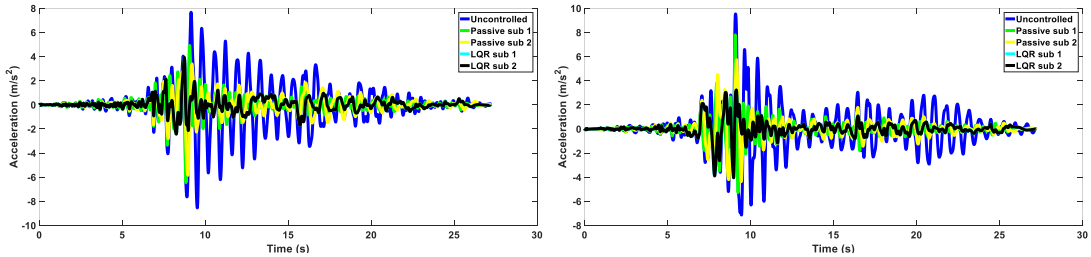

Figure 6.10: Roof acceleration a) X dir; b) Y dir subjected to record 2

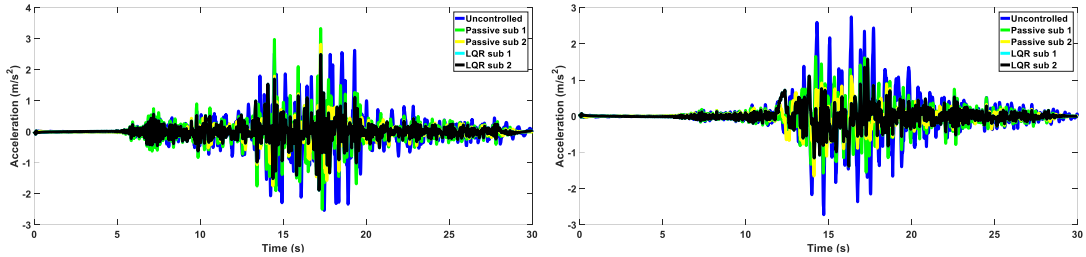

Figure 6.11: Roof acceleration a) X dir; b) Y dir subjected to record 3

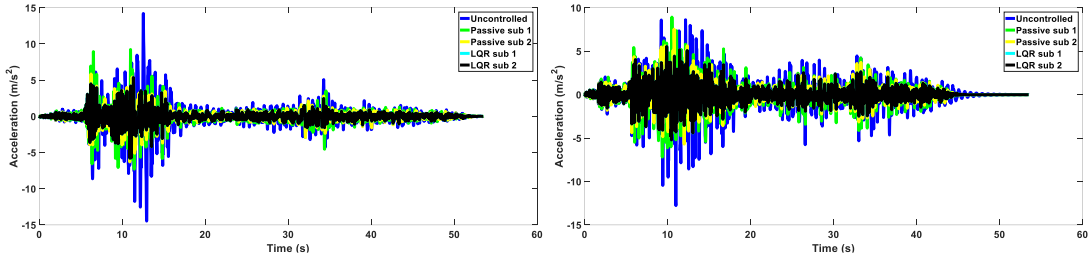

Figure 6.12: Roof acceleration a) X dir; b) Y dir subjected to record 4

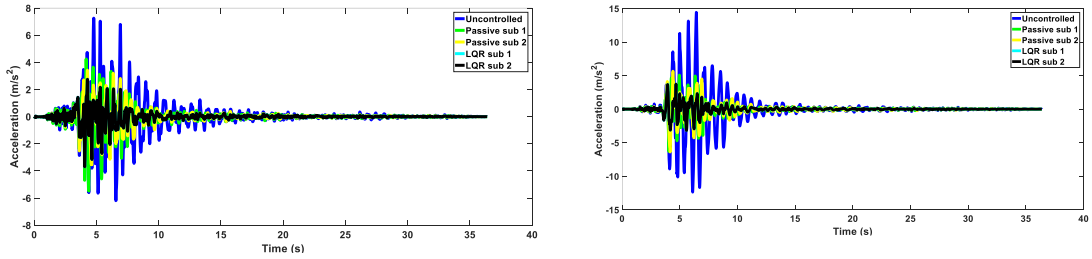

Figure 6.13: Roof acceleration a) X dir; b) Y dir subjected to record 5

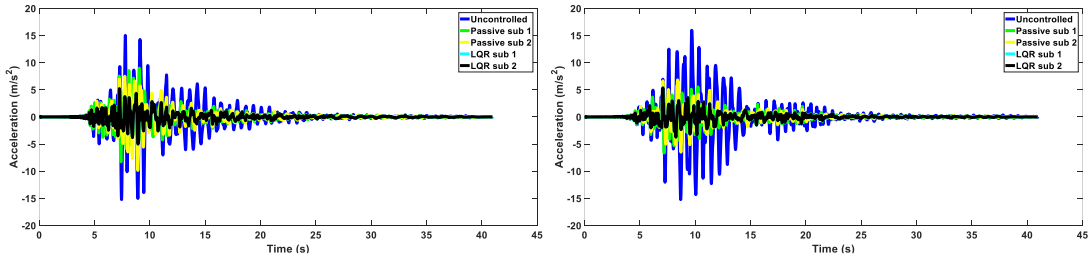

Figure 6.14: Roof acceleration a) X dir; b) Y dir subjected to record 6

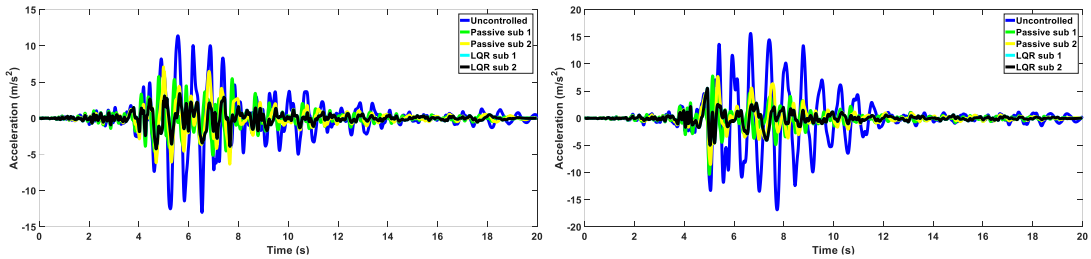

Figure 6.15: Roof acceleration a) X dir; b) Y dir subjected to record 7

Table 6.3: Max roof acceleration X dir

Record	Uncontrolled	Passive Sub 1	Passive Sub 2	LQR Sub 1	LQR Sub 2
1	19.2087	12.6035	8.9596	7.2530	7.5782
2	8.5489	6.4534	5.8476	3.9265	2.7824
3	2.6277	3.3296	2.8208	2.4937	2.2239
4	14.4654	9.2389	6.2918	5.7842	5.2175
5	7.2549	5.4819	3.5460	3.6937	3.3555
6	15.2319	8.9876	9.8697	5.2193	5.2650
7	13.0109	5.7748	7.1015	4.2247	4.0641

Table 6.4: Max roof acceleration Y dir

Record	Uncontrolled	Passive Sub 1	Passive Sub 2	LQR Sub 1	LQR Sub 2
1	17.0564	9.6179	11.8388	9.3713	8.0604
2	9.5278	7.7883	5.7458	4.0535	3.5976
3	2.7467	1.6519	1.6526	1.5814	1.2893
4	12.7710	8.9286	7.5387	5.5442	4.6927
5	14.4451	6.3184	6.3917	3.7461	3.1531
6	15.9626	6.6480	6.8236	5.3453	0.0260
7	16.8661	10.3394	8.5075	0.0124	0.0382

As it can be seen in figure 6.16 semi-active control is the best alternative to provide comfort to design and both sub-structures in both directions and for both controls had same accelration.

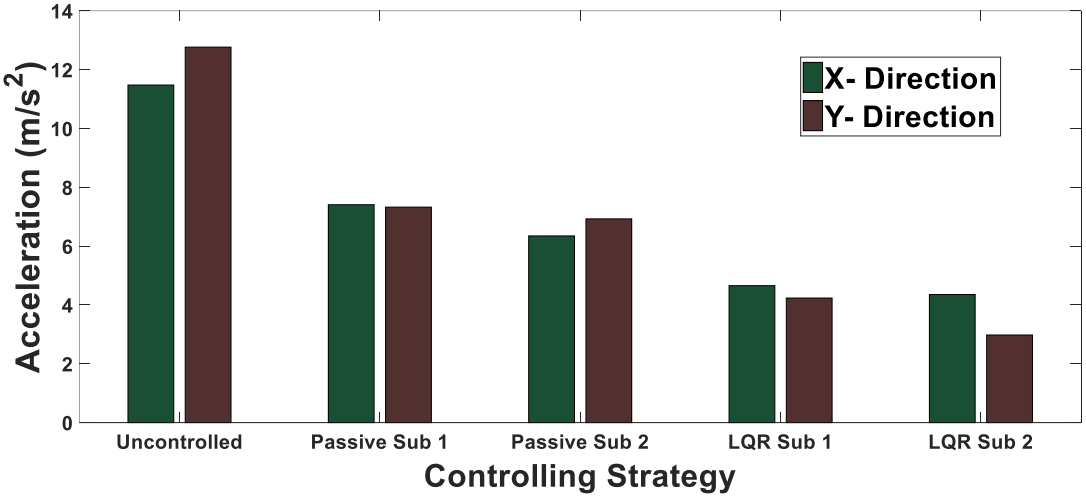

Figure 6.16: Average max acceleration regarding control and directions

The other seismic parameter investigated through the analysis was the interstory drift of the uncontrolled and passively and semi-actively controlled structures. The recommendations introduced at the Hazus can assess the damage states. The table easily depicts the passively controlled structure on average for 7 records has the interstory drift ratio of 1.0578, and 0.4522 for its soft and stiff sub-structures. Which for the soft sub-component is a little higher comparing with the uncontrolled one. On the other hand, for the semi-actively controlled sub-structure, the ratios for the interstory drifts are 0.4143, and 0.1275 respectively for the two sub-structures. The amount of maximum average interstory rotation for each case also is depicted in the bar chart below.

Table 6.5: Interstory rotation

Record	Uncontrolled	Passive Sub 1	Passive Sub 2	LQR Sub 1	LQR Sub 2

1	0.0100	0.0142	0.0061	0.0048	0.0017
2	0.0065	0.0095	0.0033	0.0033	0.0009
3	0.0020	0.0023	0.0007	0.0011	0.0002
4	0.0096	0.0076	0.0030	0.0027	0.0009
5	0.0036	0.0050	0.0027	0.0026	0.0008
6	0.0097	0.0059	0.0031	0.0026	0.0009
7	0.0088	0.0086	0.0038	0.0037	0.0010

The bar chart in figure 6.17 also reveals the soft sub-system at passive control has interstory rotation of 0.76 percent which is greater than the uncontrolled structure with 0.72 percent.

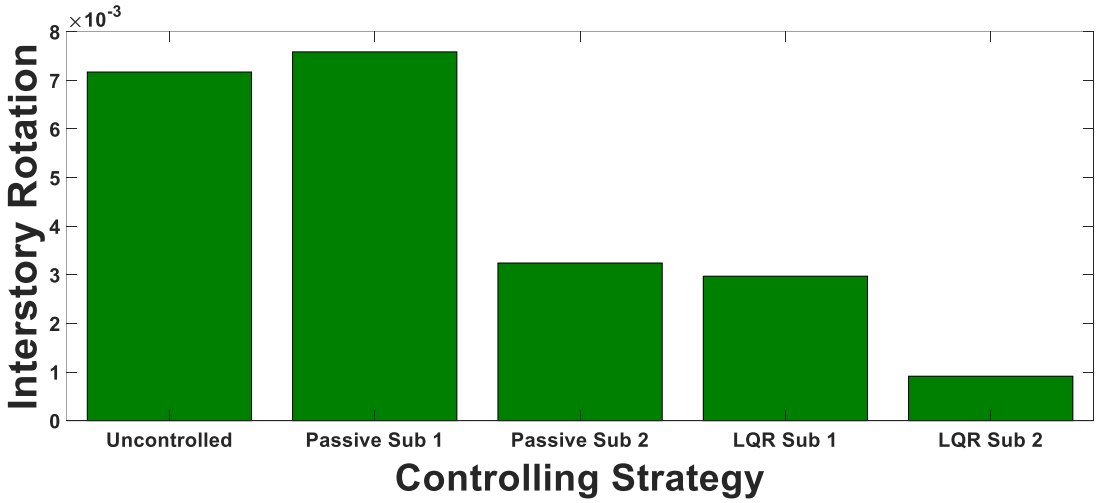

Figure 6.17: Average max interstory rotation regarding control and directions

6.2 Nine-story

The 9-story structure also expatiates the EPDs were reduced substantially like the 6-story one as the semi-active control was introduced to the system. The reduction ratios for the passive sub-structures at the X direction were 0.4260, and 0.823. These

numbers for the semi-active controlled one are 0.0922 and 0.2479. the average reduction ratios for the passive sub-structures at the Y direction are 0.5918, and 1.0329. Utilizing the semi-active control strategies reduce these ratios to 0.1061, and 0.2982 respectively.

6.2.1 Time History Displacement

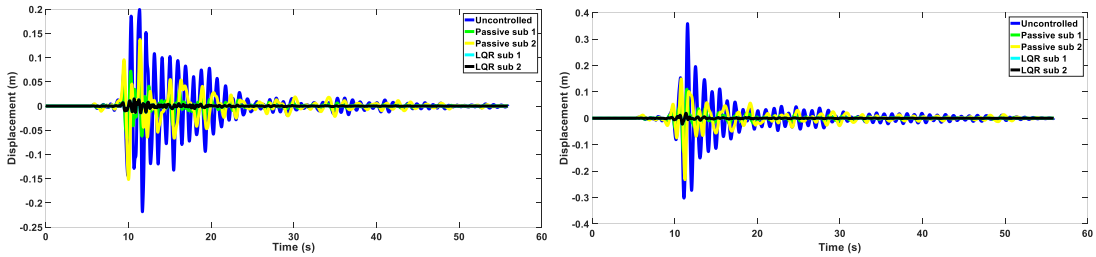

Figure 6.18: Roof displacement a) X dir; b) Y dir subjected to record 1

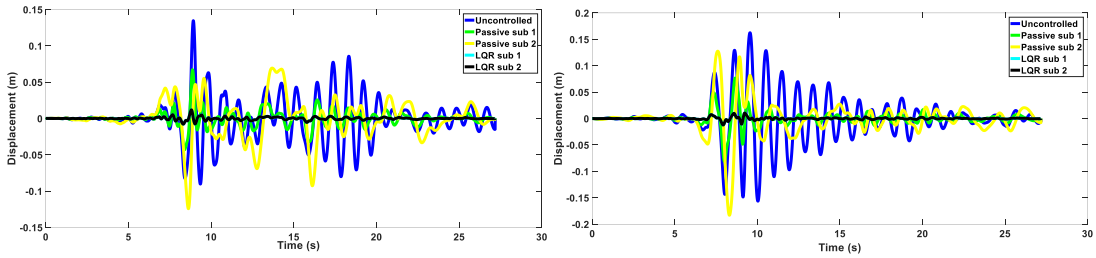

Figure 6.19: Roof displacement a) X dir; b) Y dir subjected to record 2

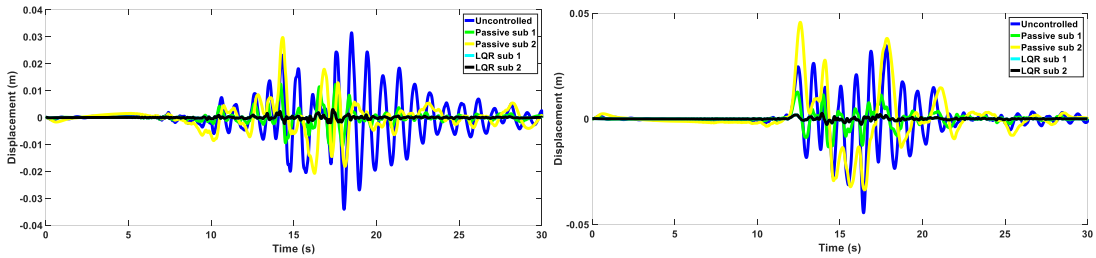

Figure 6.20: Roof displacement a) X dir; b) Y dir subjected to record 3

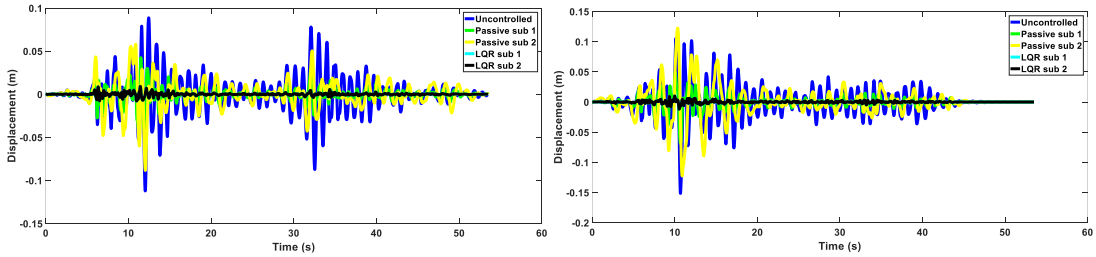

Figure 6.21: Roof displacement a) X dir; b) Y dir subjected to record 4

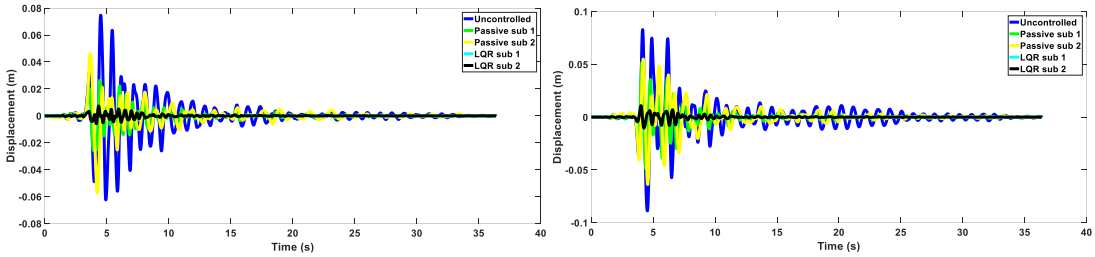

Figure 6.22: Roof displacement a) X dir; b) Y dir subjected to record 5

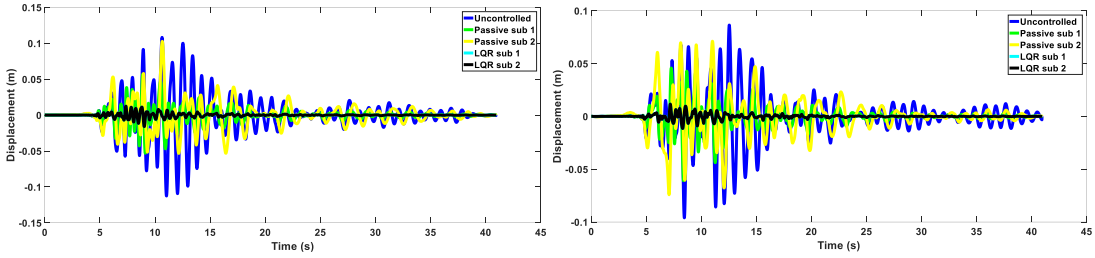

Figure 6.23: Roof displacement a) X dir; b) Y dir subjected to record 6

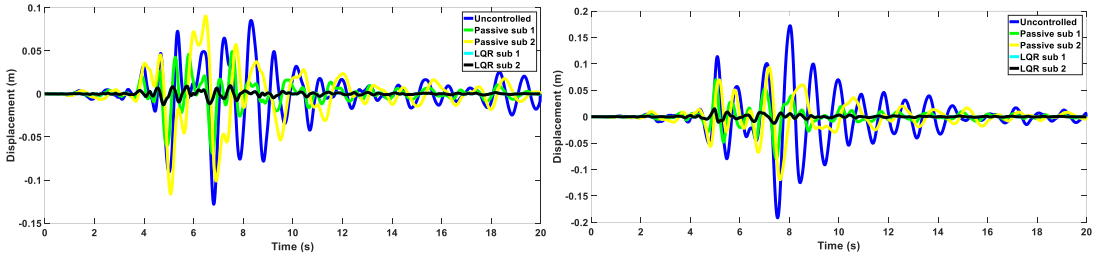

Figure 6.24: Roof displacement a) X dir; b) Y dir subjected to record 7

Table 6.6: Max roof displacement X dir

Record	Uncontrolled	Passive Sub 1	Passive Sub 2	LQR Sub 1	LQR Sub 2
1	0.2182	0.0723	0.1517	0.0150	0.0487
2	0.1346	0.0672	0.1242	0.0119	0.0343
3	0.0341	0.0127	0.0297	0.0030	0.0100
4	0.1122	0.0425	0.0884	0.0091	0.0280
5	0.0748	0.0264	0.0574	0.0074	0.0180
6	0.1126	0.0568	0.1027	0.0160	0.0293
7	0.1281	0.0691	0.1164	0.0127	0.0336

Table 6.7: Max roof displacement Y direction

Record	Uncontrolled	Passive Sub 1	Passive Sub 2	LQR Sub 1	LQR Sub 2
1	0.2182	0.1272	0.2326	0.0222	0.0646
2	0.1346	0.0809	0.1831	0.0121	0.0450
3	0.0341	0.0133	0.0457	0.0027	0.0137
4	0.1122	0.0684	0.1226	0.0119	0.0326
5	0.0748	0.0517	0.0638	0.0108	0.0226
6	0.1126	0.0608	0.0742	0.0117	0.0267
7	0.1281	0.0798	0.1194	0.0150	0.0377

The bar chart in figure 6.25 delineates the average maximum roof displacement in both directions. The soft sub-structure with 12.02 cm displacement has a greater amount compared with the uncontrolled one with11.64 cm. on the other hand, the soft sub-system at the semi-active method had a 3.47 cm maximum average displacement at the roof.

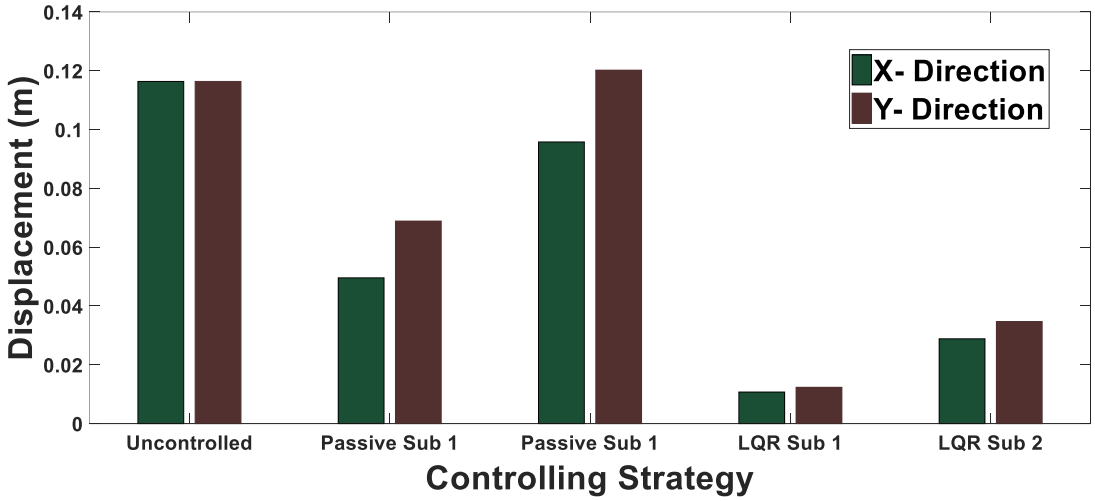

Figure 6.25: Average max displacement regarding control and directions

6.2.2 Time History Acceleration

The time history acceleration graph of the nine-story building delineates the roof accretion reduced especially by utilizing the semi-active control. The ratio of the max average accretion for soft, and stiff sub- structures subjected to the 7 bidirectional records for the passive control are 0.7338, and 0.5853 respectively. These ratios for the semi- actively controlled structure are 0.4970, and 0.4242 respectively.

These numbers for the Y direction are reduced more than the X direction which are equal to 0.6555, and 0.5595 for the passive sub-structures. For the semi- actively controlled structure the ratios are 0.4762, and 0.3793 respectively.

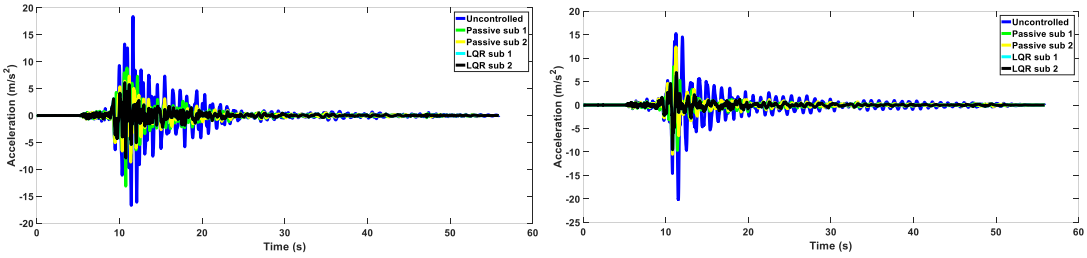

Figure 6.26: Roof acceleration a) X dir; b) Y dir subjected to record 1

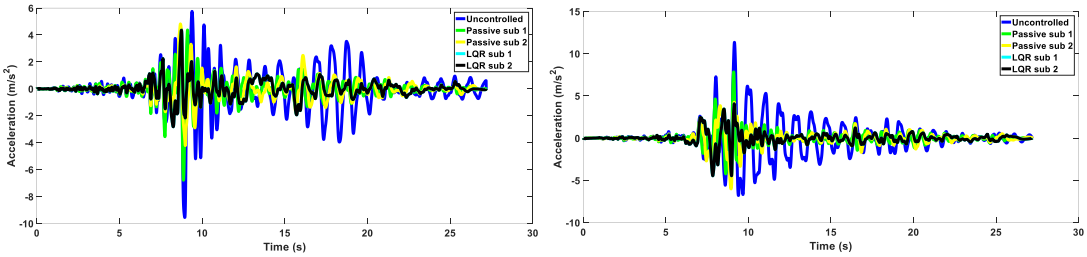

Figure 6.27: Roof acceleration a) X dir; b) Y dir subjected to record 2

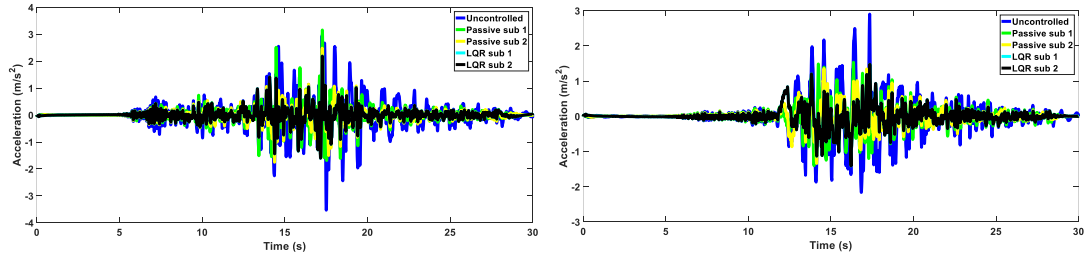

Figure 6.28: Roof acceleration a) X dir; b) Y dir subjected to record 3

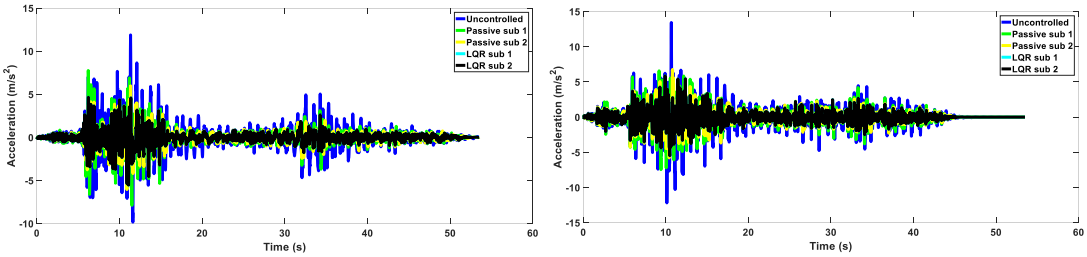

Figure 6.29: Roof acceleration a) X dir; b) Y dir subjected to record 4

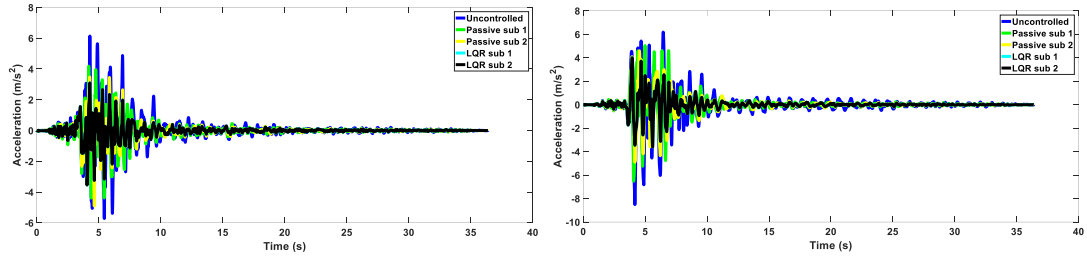

Figure 6.30: Roof acceleration a) X dir; b) Y dir subjected to record 5

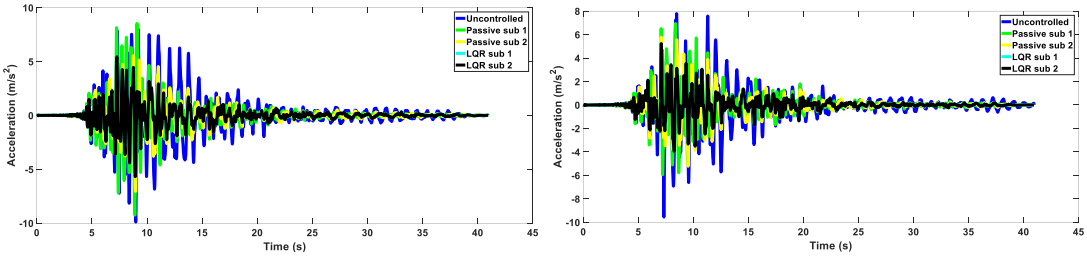

Figure 6.31: Roof acceleration a) X dir; b) Y dir subjected to record 6

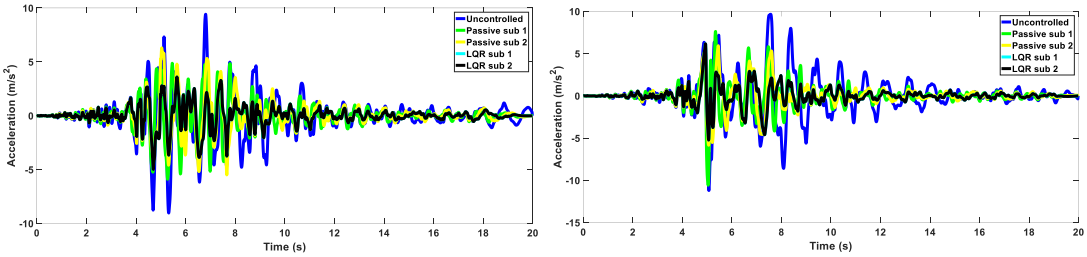

Figure 6.32: Roof acceleration a) X dir; b) Y dir subjected to record 7

Table 6.8: Max roof acceleration X dir

Record	Uncontrolled	Passive Sub 1	Passive Sub 2	LQR Sub 1	LQR Sub 2
1	18.3769	13.1118	8.6424	7.8944	7.2374
2	9.5549	6.7878	4.8245	4.3580	2.8414
3	3.5315	3.1587	2.4844	2.1889	2.1224

4	11.8883	7.8819	6.0522	5.5337	5.0765
5	6.1377	4.3904	4.9091	3.5410	3.3487
6	9.8997	9.2582	7.0623	5.6859	4.8468
7	9.4176	5.8989	6.2946	4.9942	3.7151

Table 6.9: Max roof acceleration Y dir

Record	Uncontrolled	Passive Sub 1	Passive Sub 2	LQR Sub 1	LQR Sub 2
1	20.1256	9.6604	12.3885	9.5134	7.6793
2	11.3504	7.8447	6.0068	4.4524	3.5861
3	2.9046	1.5365	1.3596	1.4790	1.2098
4	13.4396	7.4580	6.7489	5.8696	4.5910
5	8.5173	6.5224	4.9022	3.9997	2.8601
6	9.5532	6.9396	5.7867	5.2272	4.6622
7	11.2064	10.5790	5.9403	6.1698	4.6568

The acceleration response for the 9-story building shows that the 6-story building witnessed a larger amount of reduction in the response when compared with the 9-story one. The bar chart in figure 6.33 also portrays the two sub-systems have the same behavior.

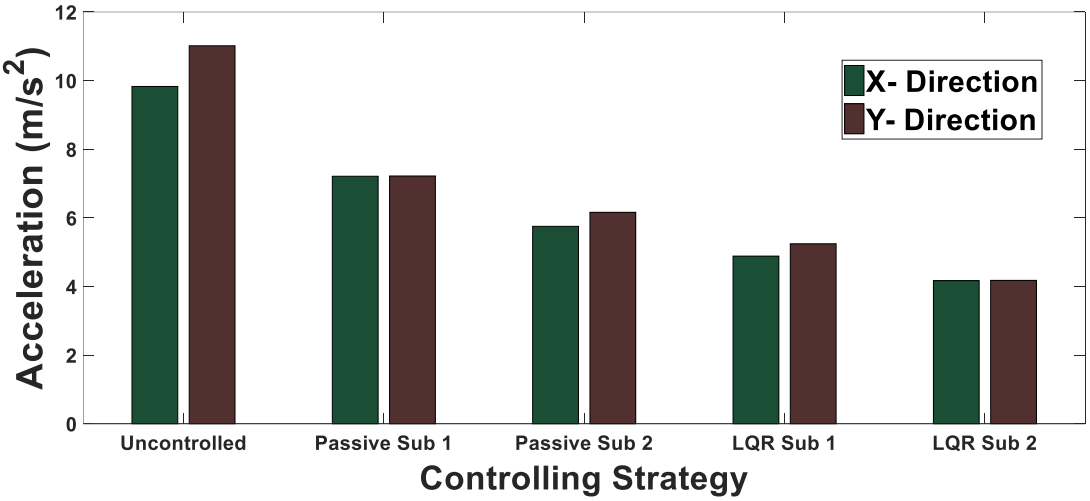

Figure 6.33: Average max acceleration regarding control and directions

Table 6.10: Interstory rotation

Record	Uncontrolled	Passive Sub 1	Passive Sub 2	LQR Sub 1	LQR Sub 2
1	0.0143	0.0112	0.0067	0.0044	0.0015
2	0.0065	0.0105	0.0043	0.0033	0.0007
3	0.0016	0.0025	0.0008	0.0011	0.0002
4	0.0057	0.0075	0.0039	0.0025	0.0008
5	0.0045	0.0043	0.0026	0.0025	0.0007
6	0.0059	0.0052	0.0031	0.0024	0.0008
7	0.0061	0.0065	0.0042	0.0035	0.0010

Interstory drift as the parameter demonstrating the column rotation and the damage state also showed a substantial reduction. The passively controlled structure on average for 7 records has the interstory drift ratio of 1.0695, and 0.5740 for its soft and stiff sub-structures. Which for the soft sub-component is a little higher compared with the uncontrolled one. On the other hand, for the semi- actively controlled sub-structure the ratios for the interstory drifts are 0.4417, and 0.1278 respectively for the two sub-

structures. As it can be seen in the bar chart below the passive soft sub-system has 0.68 percent interstory rotation greater than the uncontrolled one by 0.64 percent.

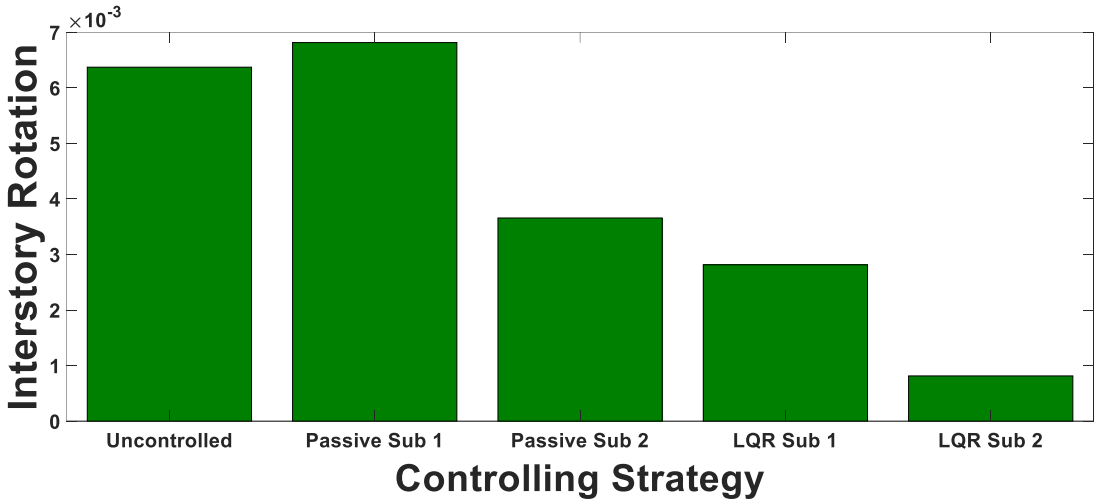

Figure 6.34: Average max interstory rotation regarding control and directions

6.3 Twelve-Story Building

6.3.1 Time History Displacement

The 12-story structure also expatiates the EPDs were reduced substantially like the 6, 9 story ones as the semi-active control was introduced to the system. The reduction ratios for the passive sub-structures at the X direction were 0.5823, and 1.0451. these numbers for the semi-active controlled one are 0.0976 and 0.2724. the result shows the amount of reduction is less than the 9 and 6-story buildings and the ratio for the soft sub-structure is more than one. On the other hand, utilizing the semi-active control reduces both sub-structure's maximum roof displacement subjected to 7 records. The average reduction ratios for the passive sub-structures at the Y-direction are 0.4947, and 0.8024. utilizing the Semi-active control strategies reduces the ratio to 0.1672, and 0.2035 respectively.

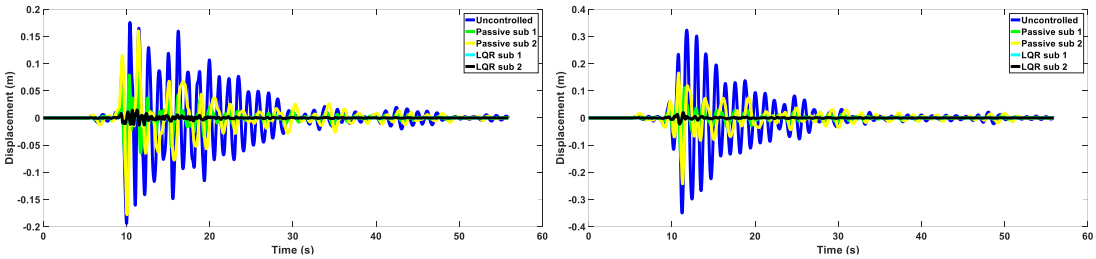

Figure 6.35: Roof displacement a) X dir; b) Y dir subjected to record 1

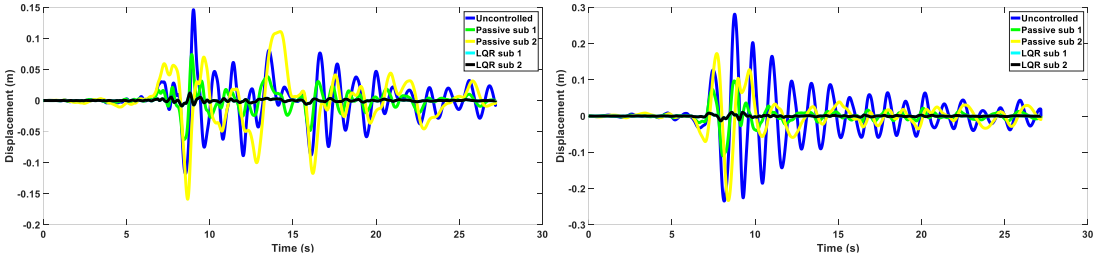

Figure 6.36: Roof displacement a) X dir; b) Y dir subjected to record 2

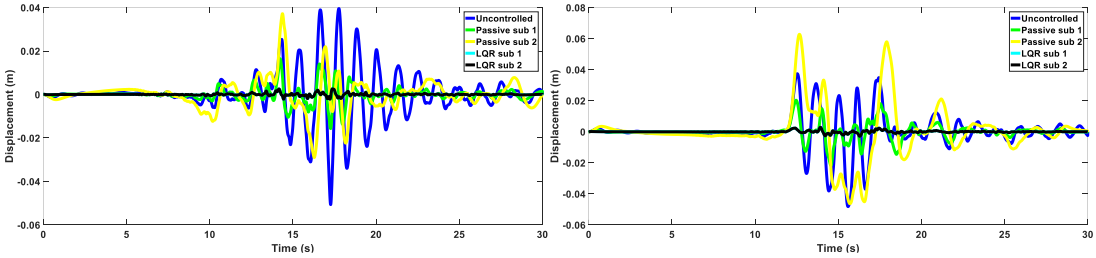

Figure 6.37: Roof displacement a) X dir; b) Y dir subjected to record 3

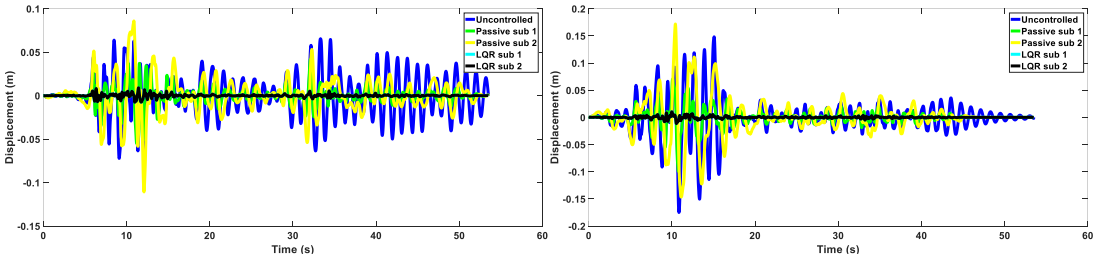

Figure 6.38: Roof displacement a) X dir; b) Y dir subjected to record 4

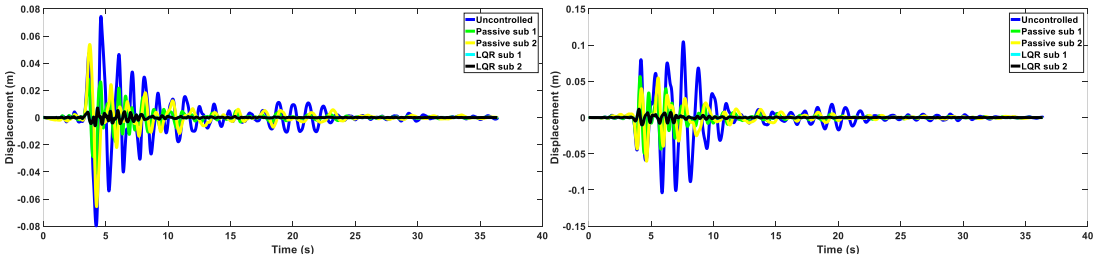

Figure 6.39: Roof displacement a) X dir; b) Y dir subjected to record 5

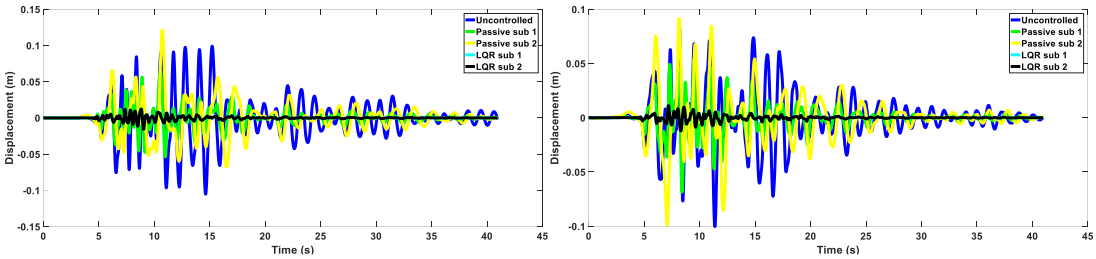

Figure 6.40: Roof displacement a) X dir; b) Y dir subjected to record 6

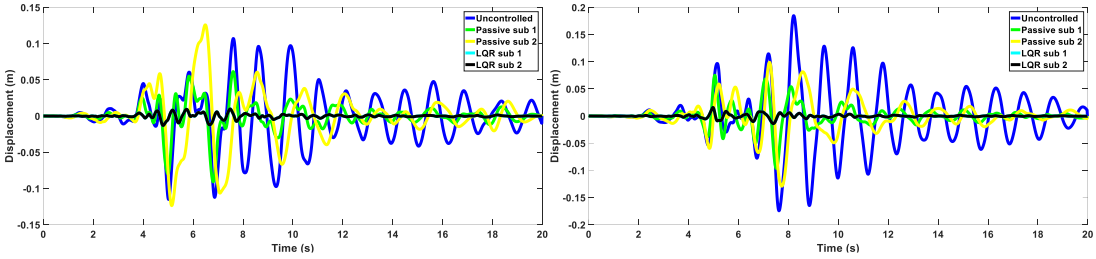

Figure 6.41: Roof displacement a) X dir; b) Y dir subjected to record 7

Table 6.11: Max roof displacement X dir

Record	Uncontrolled	Passive Sub 1	Passive Sub 2	LQR Sub 1	LQR Sub 2
1	0.1942	0.1020	0.1781	0.0146	0.0495
2	0.1463	0.0743	0.1589	0.0124	0.0370
3	0.0507	0.0165	0.0372	0.0026	0.0108
4	0.0722	0.0548	0.1108	0.0091	0.0291
5	0.0797	0.0410	0.0656	0.0071	0.0186
6	0.1053	0.0652	0.1214	0.0157	0.0290
7	0.1151	0.0908	0.1259	0.0130	0.0340

Table 6.12: Max roof displacement Y dir

Record	Uncontrolled	Passive Sub 1	Passive Sub 2	LQR Sub 1	LQR Sub 2
1	0.3500	0.1633	0.2426	0.0495	0.0637
2	0.2813	0.1096	0.2331	0.0370	0.0494
3	0.0482	0.0216	0.0627	0.0108	0.0159

4	0.1751	0.0994	0.1718	0.0291	0.0373
5	0.1045	0.0566	0.0603	0.0186	0.0214
6	0.1004	0.0686	0.0989	0.0290	0.0290
7	0.1848	0.0964	0.1289	0.0340	0.0365

The bar chart in figure 6.42 delineates the average maximum roof displacement in both directions. The uncontrolled structure with 17.78 cm has the greatest maximum average roof displacement. the soft sub- system at the passive and semi- active control has 14.26 and 3.26 cm respectively. These numbers for the stiff one at both controls are equal to 8.79 and 3.62 cm respectively.

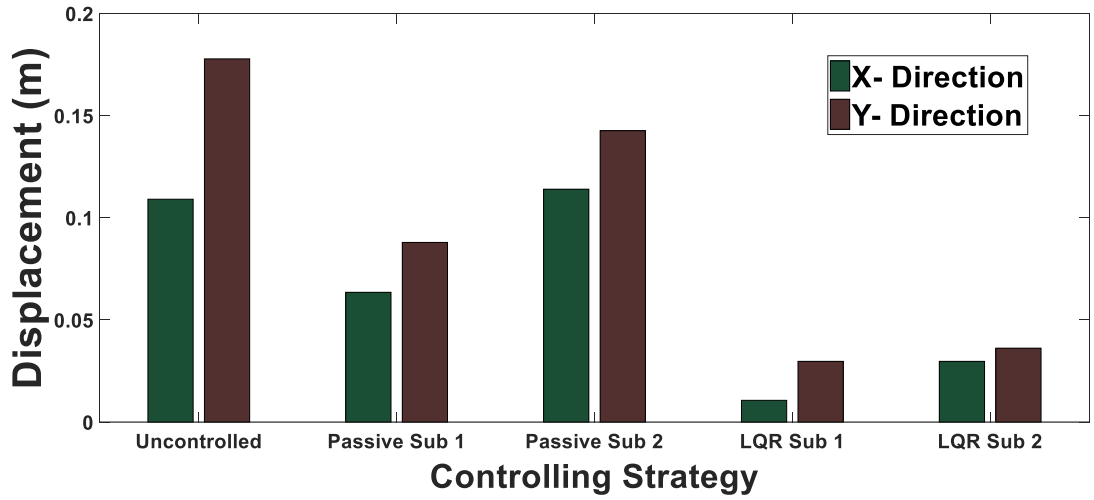

Figure 6.42: Average max displacement regarding control and directions

6.3.2 Time History Acceleration

The time history acceleration graph of the nine-story building delineates the roof accretion reduced especially by utilizing the semi-active control. The ratios of the max average acceleration for soft, and stiff sub- structures subjected to the 7 bidirectional records for the passive control are 0.7531, and 0.5935 respectively. These ratios for

the semi- actively controlled structure are 0.5454, and 0.4855 respectively. These numbers for the Y-direction are equal to 0.7993, and 0.7259 for the passive sub-structures. For the semi- actively controlled structure the ratios are 0.5871, and 0.4806 respectively.

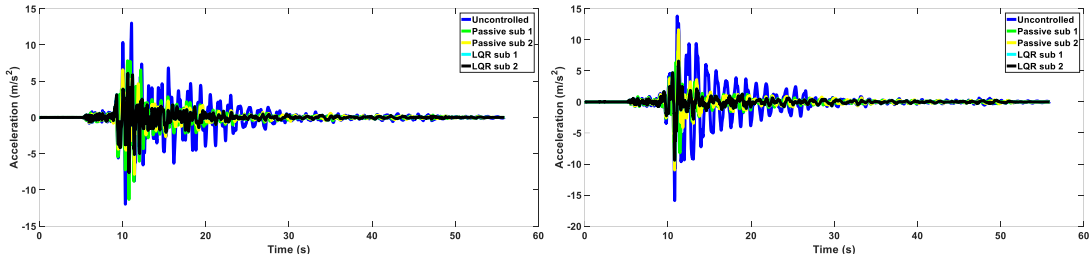

Figure 6.43: Roof acceleration a) X dir; b) Y dir subjected to record 1

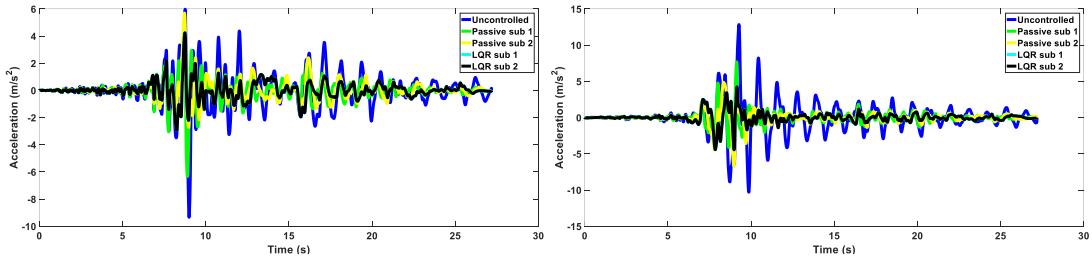

Figure 6.44: Roof acceleration a) X dir; b) Y dir subjected to record 2

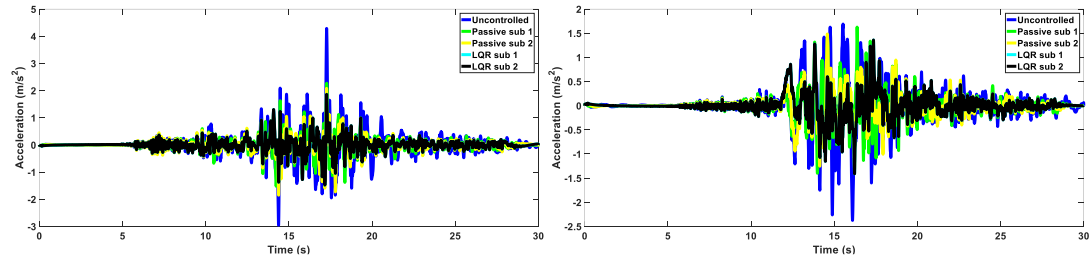

Figure 6.45: Roof acceleration a) X dir; b) Y dir subjected to record 3

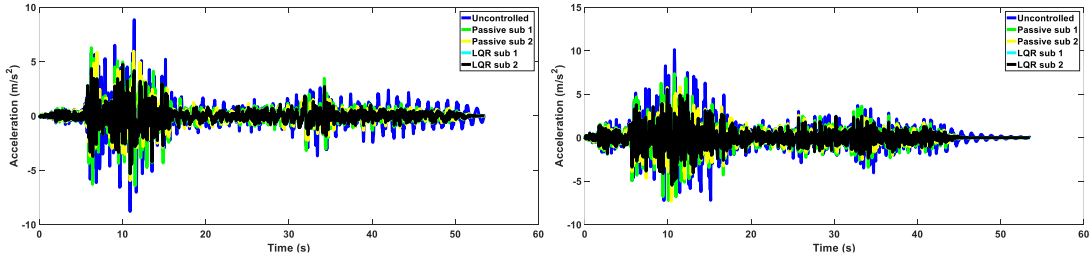

Figure 6.46: Roof acceleration a) X dir; b) Y dir subjected to record 4

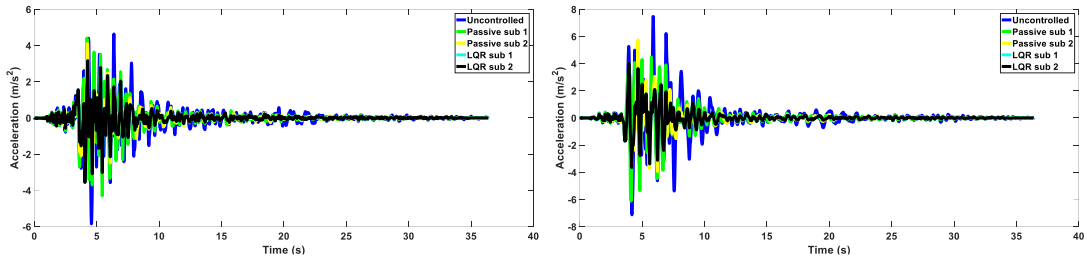

Figure 6.47: Roof acceleration a) X dir; b) Y dir subjected to record 5

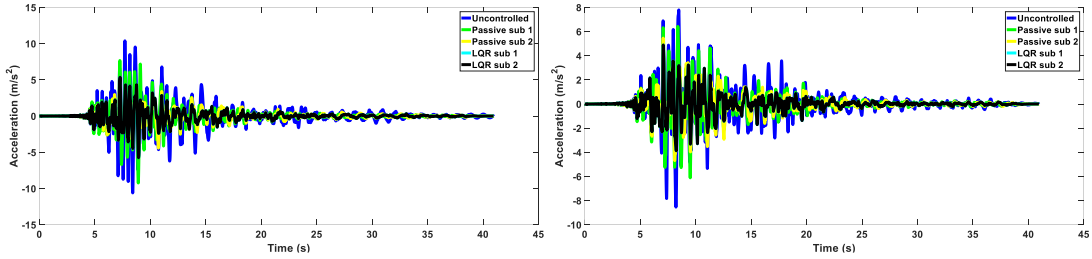

Figure 6.48: Roof acceleration a) X dir; b) Y dir subjected to record 6

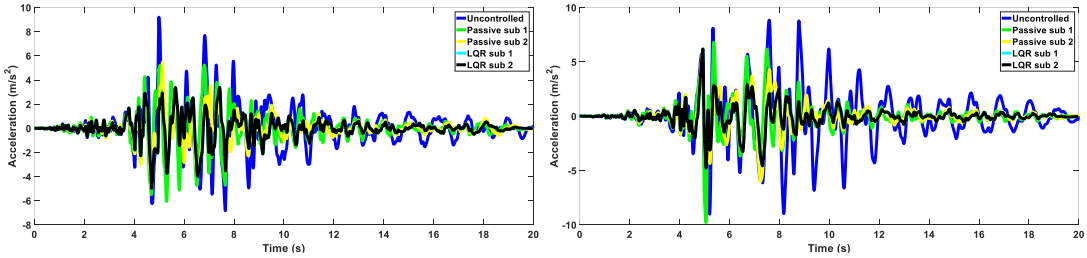

Figure 6.49: Roof acceleration a) X dir; b) Y dir subjected to record 7

Table 6.13: Max roof acceleration X dir

Record	Uncontrolled	Passive Sub 1	Passive Sub 2	LQR Sub 1	LQR Sub 2
1	13.0257	11.3173	7.8583	7.6380	7.3963
2	9.3397	6.3368	5.6976	4.2448	2.9359
3	4.2881	2.2710	2.0818	1.8619	2.0851
4	8.8526	6.4265	5.9570	5.3238	5.0665
5	5.8491	4.4124	4.1101	3.5634	3.4685
6	10.6038	9.2320	5.1161	5.7529	4.8749
7	9.2002	6.0633	5.4773	4.9706	3.8648

Table 6.14: Max roof acceleration Y dir

Record	Uncontrolled	Passive Sub 1	Passive Sub 2	LQR Sub 1	LQR Sub 2
1	13.0257	9.9028	11.6271	9.3895	7.7583
2	9.3397	7.6875	6.7610	4.4425	3.5969
3	4.2881	1.6269	1.4847	1.4114	1.2496
4	8.8526	7.3525	7.3153	5.5415	4.5905
5	5.8491	6.1175	5.7429	4.0404	2.9751
6	10.6038	6.4241	5.4579	4.8891	4.6252
7	9.2002	9.7758	6.0048	6.1926	4.5986

The bar chart in figure 6.50 also portrays similar to the 9-story building the two sub-systems at both controls have the same behavior.

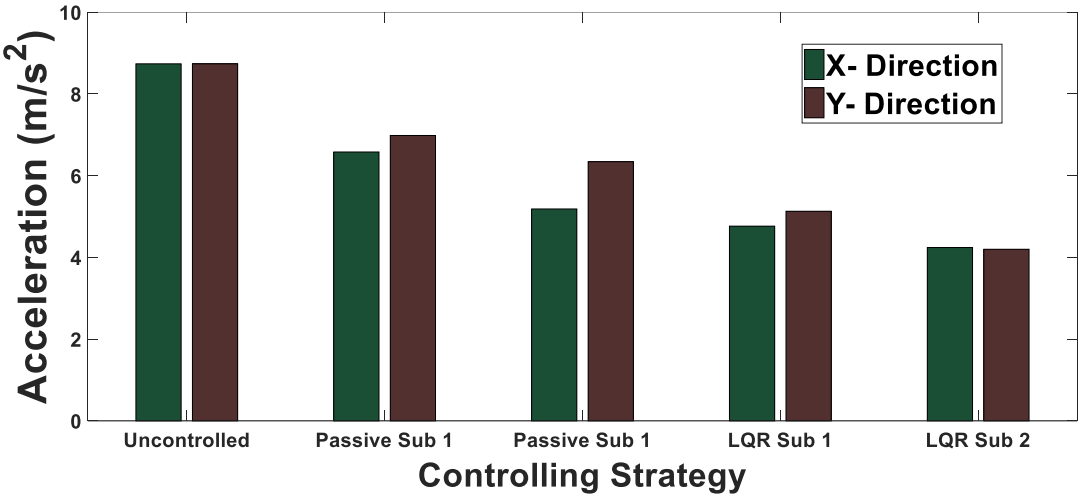

Figure 6.50: Average max acceleration regarding control and directions

Table 6.15: Interstory rotation

Record	Uncontrolled	Passive Sub 1	Passive Sub 2	LQR Sub 1	LQR Sub 2
1	0.0086	0.0094	0.0065	0.0042	0.0014
2	0.0057	0.0101	0.0044	0.0031	0.0007

3	0.0020	0.0027	0.0009	0.0011	0.0002
4	0.0041	0.0077	0.0042	0.0024	0.0007
5	0.0044	0.0039	0.0022	0.0024	0.0006
6	0.0042	0.0057	0.0026	0.0023	0.0007
7	0.0045	0.0058	0.0036	0.0034	0.0009

The passively controlled structure on average for 7 records has the interstory drift ratio of 1.3522, and 0.7284 for its soft and stiff sub-structures. Which for the soft sub-component is higher compared with the uncontrolled one. On the other hand, for the semi-actively controlled sub-structure the ratio for the interstory drifts are 0.5642, and 0.1552 respectively for the two sub-structures.

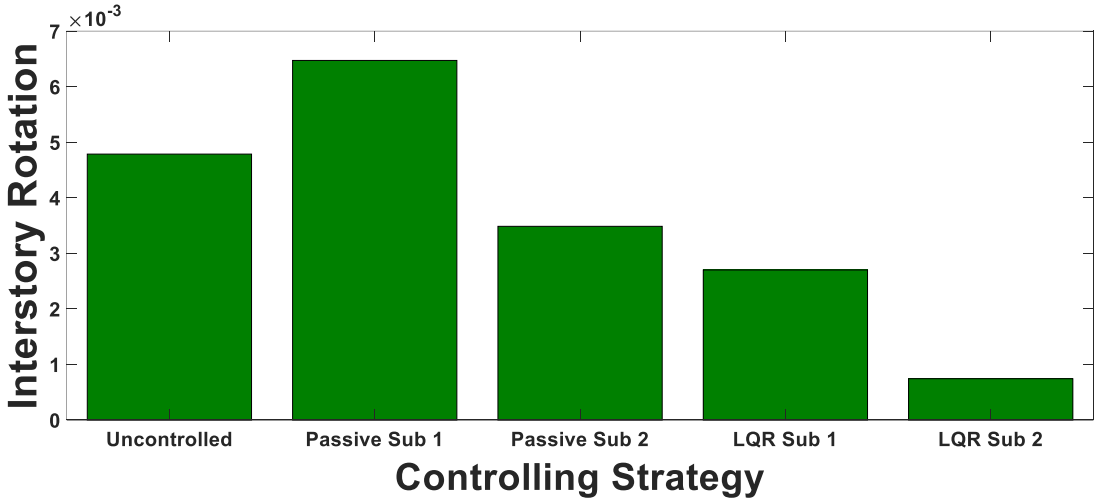

Figure 6.51: Average max interstory rotation regarding control and directions

Chapter 7

CONCLUSION AND SUGGESTIONS

7.1 Conclusion

In this study 6,9 and 12-story buildings by considering three-dimensional modeling were subjected to 7 bidirectional ground motions. Each structure was investigated without vertical isolation, with passive vertical isolation, and finally with semi-active vertical isolation with an MR damper. The results for all structures delineate that passive vertical isolation can reduce the roof displacement and acceleration for the stiff sub-structure. On the other hand, the soft sub-structure is sensitive to the selected ground motion. The semi-active control of the structure however was able to reduce sub-structure maximum roof displacement, acceleration, and interstory drift. The controlling strategies portrayed prominent response reduction for acceleration even for the passive case. On the other hand, the semi-active strategy is the only control method that reduced the displacement and the interstory drift by greater measures:

- The maximum roof displacement for the 6, 9, and 12- story on average for the inner and outer sub-systems are 46.79 and 86.87 percent of the uncontrolled one. The semi-active control on the other hand reduced displacements to 9.92 and 28.44 percent on average.
- The average maximum roof acceleration of the buildings for the inner and outer sub- systems are 59.33 and 69.35 percent of the uncontrolled one. However, the acceleration as the semi-active control is used dropped to 39.71 and 47.39.

- The average maximum interstory rotation of the sub-systems at 6, 9, and 12-story buildings are 58.5 and 116 percent of the uncontrolled one. The semi-active control was able to decrease it to 13.68, and 47.34.

7.2 Suggestion

1. A greater number of seismic records can be used to study the sensitivity of the response to ground motions.
2. Other control strategies such as SAC, Lyaponouv, and sliding mode control can be used to investigate the feasibility of each record.
3. Investigating the damper placement effect for cost reduction and having an optimized response reduction.
4. Finding an optimized mass and stiffness ratio for sub-structures regarding a number of records and investigating the applicability of the ratio when the structure is subjected to other records set.
5. Assess the effect of uncertainty in response utilizing probabilistic analysis and the Monte Carlo method.

REFERENCES

[1] S. Sefidkar-Dezfouli, "Design, simulation, and fabrication of a lightweight magneto rheological damper," Simon Fraser University, March 5, 2014

[2] C. E. Mortimer, "Introduction to Chemistry", 5th edition ed. Belmont, Calif, Wadsworth Pub. Co, 1983.

[3] Y. Lu, "Development of an energy-harvesting magnetorheological fluid damper development of an energy-harvesting magnetorheological," 2016.

[4] A. J. D. Nanthakumar, J. Jancirani, S. C. Rajasekaran, and K. Sarathkumar, "Multiphysics analysis of a magnetorheological damper," vol. 69, no. 3, pp. 230-235, 2019.

[5] "Manual for structural damping systems in design and retrofitting of buildings", Housing and Urban Development Research Center of Iran, 2018.

[6] H. A. Metered, "Modelling and control of magnetorheological dampers for vehicle suspension systems," 2010.

[7] J. Poynor, "Innovative designs for magneto-rheological dampers," Master, Mechanical Engineering Advanced Vehicle Dynamics Laboratory Virginia Polytechnic Institute and State University, Advanced Vehicle Dynamics Laboratory Virginia Polytechnic Institute and State University, 2001.

[8] G. L. a. T. L. Yangguang Xu. "Magneto-sensitive smart materials and magnetorheological mechanism." https://www.intechopen.com/chapters/66109.

[9] N. Hoang, N. Zhang, and H. Du, "A dynamic absorber with a soft magnetorheological elastomer for powertrain vibration suppression," *Smart Materials and Structures,* vol. 18, no. 7, p. 074009, 2009/06/15 2009, doi: 10.1088/0964-1726/18/7/074009.

[10] H.-x. Deng and X.-l. Gong, "Application of magnetorheological elastomer to vibration absorber," *Communications in Nonlinear Science and Numerical Simulation,* vol. 13, no. 9, pp. 1938-1947, 2008/11/01/ 2008, doi: https://doi.org/10.1016/j.cnsns.2007.03.024.

[11] Q. Wang, X. Dong, L. Li, and J. Ou, "Mechanical modeling for magnetorheological elastomer isolators based on constitutive equations and electromagnetic analysis," *Smart Materials and Structures,* vol. 27, no. 6, p. 065017, 2018/05/08 2018, doi: 10.1088/1361-665x/aabdb5.

[12] J. Yang, "Development of magnetorheological elastomer technologies for protecting structures from seismic events," Doctor of Philosophy, Mechanical, Materials & Mechatronic, University of Wollongong, 2016.

[13] A. K. Bastola and M. Hossain, "A review on magneto-mechanical characterizations of magnetorheological elastomers," *Composites Part B:*

Engineering, vol. 200, p. 108348, 2020/11/01/ 2020, doi: https://doi.org/10.1016/j.compositesb.2020.108348.

[14] S. Ali, A. Suresh, and N. Seetharamaiah, "Principles , characteristics and applications of magneto rheological fluid damper in flow and shear mode," *Procedia Materials Science,* vol. 6, no. Icmpc, pp. 1547-1556, 2014, doi: 10.1016/j.mspro.2014.07.136.

[15] A. G. Olabi and A. Grunwald, "Design and application of magneto-rheological fluid," *Materials & Design,* vol. 28, no. 10, pp. 2658-2664, 2007/01/01/ 2007, doi: https://doi.org/10.1016/j.matdes.2006.10.009.

[16] M. Rahman, Z. C. Ong, S. Julai, M. Ferdaus, and R. Ahamed, "A review of advances in magnetorheological dampers : their design optimization and applications," vol. 18, no. 12, pp. 991-1010, 2017.

[17] O. A. S. Al-Fahdawi, L. R. Barroso, and R. W. Soares, "Simple adaptive control method for mitigating the seismic responses of coupled adjacent buildings considering parameter variations," *Engineering Structures,* vol. 186, pp. 369-381, 2019/05/01/ 2019, doi: https://doi.org/10.1016/j.engstruct.2019.02.025.

[18] O. A. S. Al-Fahdawi, L. R. Barroso, and R. W. Soares, "Semi-active adaptive control for enhancing the seismic performance of nonlinear coupled buildings with smooth hysteretic behavior," *Engineering Structures,* vol. 191, pp. 536-548, 2019/07/15/ 2019, doi: https://doi.org/10.1016/j.engstruct.2019.04.078.

[19] A. Yanik and U. Aldemir, "A simple structural control model for earthquake excited structures," *Engineering Structures,* vol. 182, pp. 79-88, 2019/03/01/ 2019, doi: https://doi.org/10.1016/j.engstruct.2018.12.075.

[20] X. Guan, J. Zhang, H. Li, and J. Ou, "Semi-active control for benchmark building using innovative tmd with mre isolators," *International Journal of Structural Stability and Dynamics,* vol. 20, no. 06, p. 2040009, 2020/06/01 2020, doi: 10.1142/S021945542040009X.

[21] M. B. a. F. Khoshnoudian, "The effect of impact with adjacent structure on seismic behavior of base-isolated buildings with DCFP bearings," *Structural Engineering and Mechanics,* vol. 51, 2014, doi: http://dx.doi.org/10.12989/sem.2014.51.2.277.

[22] W.-S. C. C. S. Tsai, Bo-Jen Chen, Wen-Shen Pong, "Vertical distributions of lateral forces on base isolated structures considering higher mode effects," *Structural Engineering and Mechanics,* 2006, doi: http://dx.doi.org/10.12989/sem.2006.23.5.543.

[23] D.-D. J. Jeong-Hoi Koo, Muhammad Usman and Hyung-Jo Jung, "A feasibility study on smart base isolation systems using magneto-rheological elastomers," *Structural Engineering and Mechanics,* vol. 32, 2009, doi: https://doi.org/10.12989/sem.2009.32.6.755.

[24] D. De Domenico, N. Impollonia, and G. Ricciardi, "Soil-dependent optimum design of a new passive vibration control system combining seismic base

isolation with tuned inerter damper," *Soil Dynamics and Earthquake Engineering,* vol. 105, pp. 37-53, 2018/02/01/ 2018, doi: https://doi.org/10.1016/j.soildyn.2017.11.023.

[25] M. De Angelis, A. Giaralis, F. Petrini, and D. Pietrosanti, "Optimal tuning and assessment of inertial dampers with grounded inerter for vibration control of seismically excited base-isolated systems," *Engineering Structures,* vol. 196, p. 109250, 2019/10/01/ 2019, doi: https://doi.org/10.1016/j.engstruct.2019.05.091.

[26] Y. Liu, J. Wu, and M. Donà, "Effectiveness of fluid-viscous dampers for improved seismic performance of inter-storey isolated buildings," *Engineering Structures,* vol. 169, pp. 276-292, 2018/08/15/ 2018, doi: https://doi.org/10.1016/j.engstruct.2018.05.031.

[27] K. Skandalos, H. Afshari, W. Hare, and S. Tesfamariam, "Multi-objective optimization of inter-story isolated buildings using metaheuristic and derivative-free algorithms," *Soil Dynamics and Earthquake Engineering,* vol. 132, p. 106058, 2020/05/01/ 2020, doi: https://doi.org/10.1016/j.soildyn.2020.106058.

[28] X. T. Ma *et al.*, "Dynamic response analysis of story-adding structure with isolation technique subjected to near-fault pulse-like ground motions," *Physics and Chemistry of the Earth, Parts A/B/C,* vol. 121, p. 102957, 2021/02/01/ 2021, doi: https://doi.org/10.1016/j.pce.2020.102957.

[29] T. C. Becker and A. Ezazi, "Enhanced performance through a dual isolation seismic protection system," *The Structural Design of Tall and Special Buildings,* vol. 25, no. 1, pp. 72-89, 2016/01/01 2016, doi: 10.1002/tal.1229.

[30] H.-S. Kim and J.-W. Kang, "Optimal design of smart mid-story isolated control system for a high-rise building," *International Journal of Steel Structures,* vol. 19, no. 6, pp. 1988-1995, 2019/12/01 2019, doi: 10.1007/s13296-019-00258-8.

[31] M. Q. F. W. Chai, "Design of a mega-sub-controlled building system under stochastic wind loads," *Prob. Engng Mech. Vol. 12, No. 3, pp. 149-162, 1997 Elsevier Science,* vol. Vol. 12, No. 3, pp. 149-162, 1997, 1997.

[32] H. Anajafi and R. A. Medina, "Comparison of the seismic performance of a partial mass isolation technique with conventional TMD and base-isolation systems under broad-band and narrow-band excitations," *Engineering Structures,* vol. 158, pp. 110-123, 2018/03/01/ 2018, doi: https://doi.org/10.1016/j.engstruct.2017.12.018.

[33] E. S. S. L. Zhidong Yang, "Seismic mitigation of an existing building by connecting to a base-isolated building with visco-elastic dampers," *Structural Engineering and Mechanics,* vol. 53, 2015, doi: https://doi.org/10.12989/sem.2014.53.1.057.

[34] M. Ziyaeifar and H. Noguchi, "Partial mass isolation in tall buildings," *Earthquake Engineering & Structural Dynamics,* vol. 27, no. 1, pp. 49-65,

1998/01/01 1998, doi: 10.1002/(SICI)1096-9845(199801)27:1<49::AID-EQE718>3.0.CO;2-J.

[35] M. Ziyaeifar, S. Gidfar, and M. Nekooei, "A model for Mass Isolation study in seismic design of structures," *Structural Control and Health Monitoring,* vol. 19, no. 6, pp. 627-645, 2012/10/01 2012, doi: 10.1002/stc.459.

[36] R. Milanchian and M. Hosseini, "Study of vertical seismic isolation technique with nonlinear viscous dampers for lateral response reduction," *Journal of Building Engineering,* vol. 23, pp. 144-154, 2019/05/01/ 2019, doi: https://doi.org/10.1016/j.jobe.2019.01.026.

[37] N. R. Fisco and H. Adeli, "Smart structures: Part I—Active and semi-active control," *Scientia Iranica,* vol. 18, no. 3, pp. 275-284, 2011/06/01/ 2011, doi: https://doi.org/10.1016/j.scient.2011.05.034.

[38] S. Thenozhi and W. Yu, "Advances in modeling and vibration control of building structures," *ANNUAL REVIEWS IN CONTROL,* 2013, doi: 10.1016/j.arcontrol.2013.09.012.

[39] S. F. Ali, "Testing and modeling of mr damper and its application to SDOF systems using integral backstepping technique," vol. 131, no. March, pp. 1-11, 2009, doi: 10.1115/1.3072154.

[40] B. F. Spencer, S. J. Dyke, M. K. Sain, and J. D. Carlson, "Phenomenological model for magnetorheological dampers," *Journal of Engineering Mechanics,*

vol. 123, no. 3, pp. 230-238, 1997/03/01 1997, doi: 10.1061/(ASCE)0733-9399(1997)123:3(230).

[41] M. Bitaraf, O. E. Ozbulut, S. Hurlebaus, and L. Barroso, "Application of semi-active control strategies for seismic protection of buildings with MR dampers," *Engineering Structures,* vol. 32, no. 10, pp. 3040-3047, 2010, doi: 10.1016/j.engstruct.2010.05.023.

[42] M. E. Uz and M. N. S. Hadi, "Optimal design of semi active control for adjacent buildings connected by MR damper based on integrated fuzzy logic and multi-objective genetic algorithm," *Engineering Structures,* vol. 69, pp. 135-148, 2014/06/15/ 2014, doi: https://doi.org/10.1016/j.engstruct.2014.03.006.

[43] T. Soong, "Active Structural Control: Theory and Practice" Department of Civil Engineering State University of New York at Buffalo, 1990.

[44] I. Barkana and J. Z. Ben-Asher, "Simple adaptive control applications to large flexible structures," *Journal of Guidance, Control, and Dynamics,* vol. 34, no. 6, pp. 1929-1932, 2011/11/01 2011, doi: 10.2514/1.54217.

[45] G. Leitmann, "Semiactive Control for Vibration Attenuation," *Journal of Intelligent Material Systems and Structures,* vol. 5, no. 6, pp. 841-846, 1994/11/01 1994, doi: 10.1177/1045389X9400500616.

[46] "*FEMA P695 Quantification of Building Seismic Performance Factors",* FEMA, 2009.

[47] B. F. Spencer Jr, S. J. Dyke, and H. S. Deoskar, "Benchmark problems in structural control: part I—Active Mass Driver system," *Earthquake Engineering & Structural Dynamics,* vol. 27, no. 11, pp. 1127-1139, 1998/11/01 1998, doi: 10.1002/(SICI)1096-9845(1998110)27:11<1127::AID-EQE774>3.0.CO;2-F.

[48] "Multi-hazard Loss Estimation Methodology Earthquake Model", FEMA, 2003.

APPENDICES

Appendix A: Bidirectional Ground Motions

In this study, 7 bidirectional records aligned with FEMA P695 provisions were selected. In the process of electing the records no scaling is introduced.

Table A. 1: X dir components of seismic records

Seismic record	Number of dots	Time step	PGA (m/s^2)
Düzce Turkey 1999	5590	0.01	7.2520
Kocaeli Turkey 1999	5437	0.005	3.0600
Kocaeli Arcelik 1999	6000	0.005	2.061
Manjil–Rudbar1990	2676	0.02	5.048
Friuli, Italy Tolmezzo 1976	7277	0.005	3.503
Kobe, Japan Nishi-Akashi 1995	4096	0.01	4.7400
Northridge Canyon Country 1994	1999	0.01	3.959

Table A. 2: Y dir components of seismic records

Seismic record	Number of dots	Time step	PGA (m/s^2)
Düzce Turkey 1999	5590	0.01	7.904
Kocaeli Turkey 1999	5437	0.005	3.573
Kocaeli Arcelik 1999	6000	0.005	1.316
Manjil–Rudbar1990	2676	0.02	4.874
Friuli, Italy Tolmezzo 1976	7277	0.005	3.091
Kobe, Japan Nishi-Akashi 1995	4096	0.01	4.555

Northridge Canyon Country 1994	1999	0.01	4.627

A.1 Düzce Turkey 1999

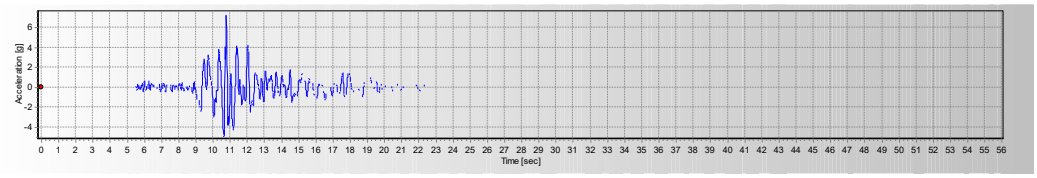

Figure A. 1: X dir of Düzce Turkey 1999

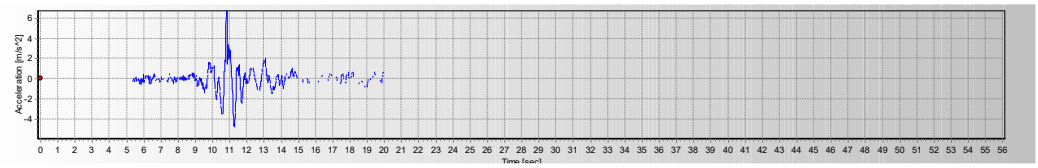

Figure A. 2: Y dir of Düzce Turkey 1999

A.2 Kocaeli Turkey 1999

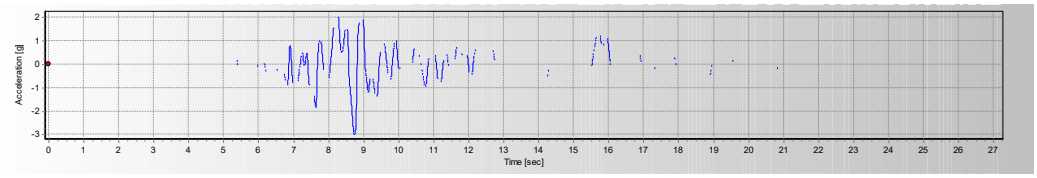

Figure A. 3: X dir of Kocaeli Turkey 1999

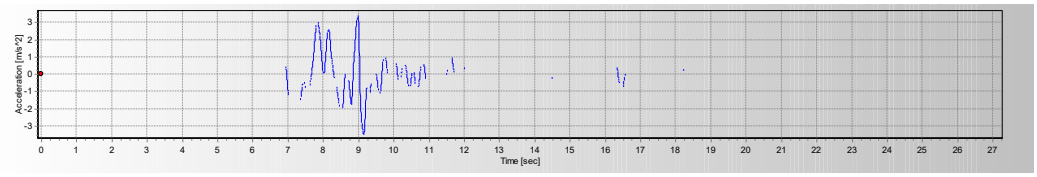

Figure A. 4: Y dir of Kocaeli Turkey 1999

A.3 Kocaeli Arcelik 1999

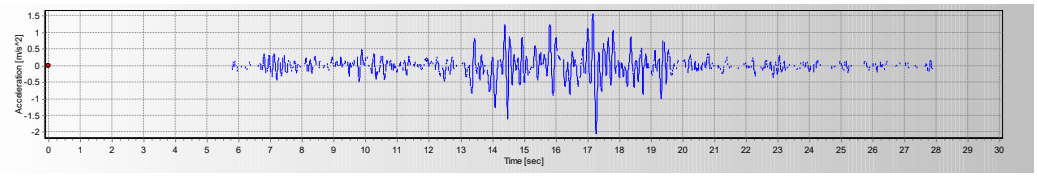

Figure A. 5: X dir of Kocaeli Arcelik 1999

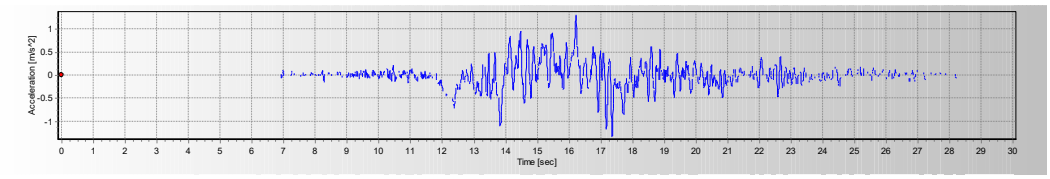

Figure A. 6: Y dir of Kocaeli Arcelik 1999

A.4 Manjil–Rudbar1990

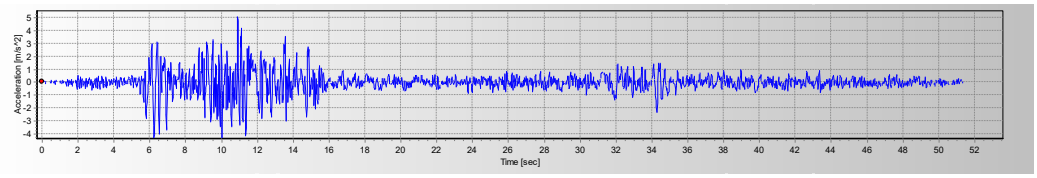

Figure A. 7: X dir of Manjil–Rudbar1990

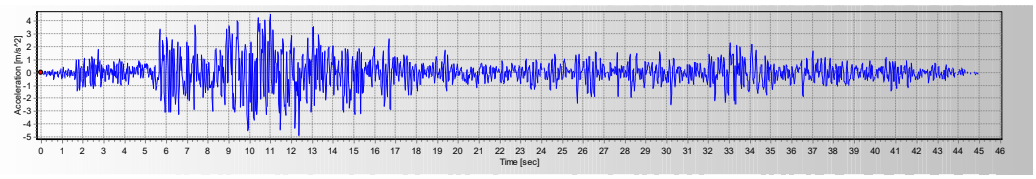

Figure A. 8: Y dir of Manjil–Rudbar1990

A.5 Friuli, Italy Tolmezzo 1976

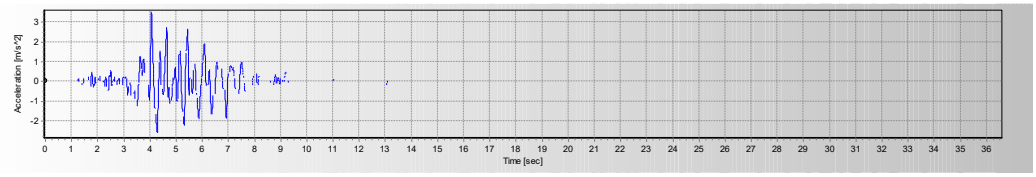

Figure A. 9: X dir of Friuli, Italy Tolmezzo 1976

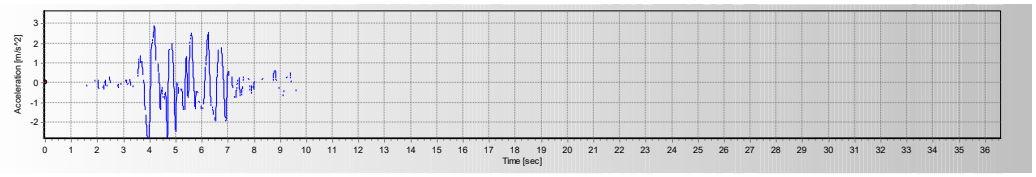

Figure A. 10: Y dir of Friuli, Italy Tolmezzo 1976

A.6 Kobe, Japan Nishi-Akashi 1995

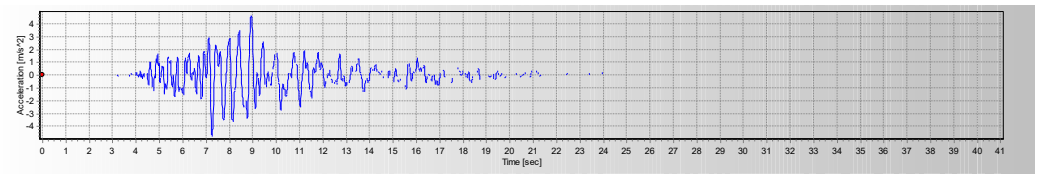

Figure A. 11: X dir of Kobe, Japan Nishi-Akashi 1995

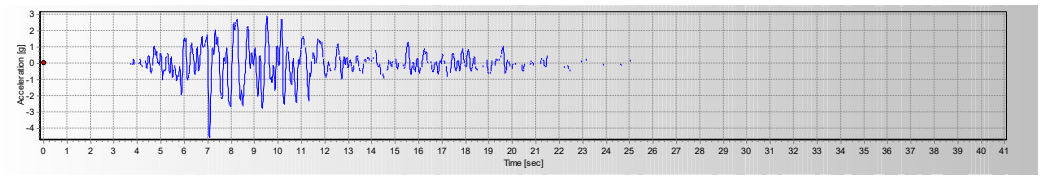

Figure A. 12: Y dir of Kobe, Japan Nishi-Akashi 1995

A.7 Northridge Canyon Country 1994

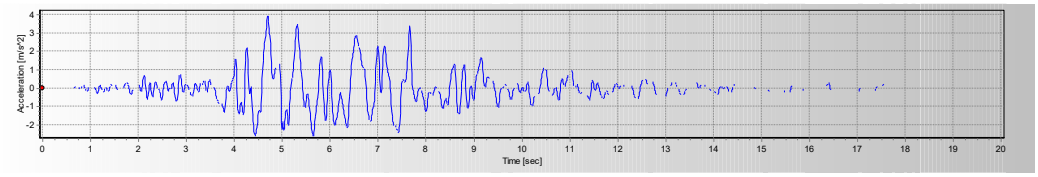

Figure A. 13: X dir of Northridge Canyon Country 1994

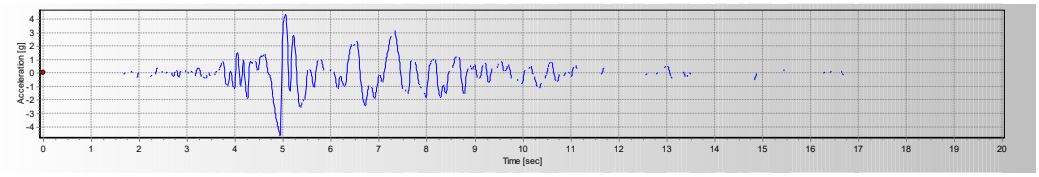

Figure A. 14 Y dir of Northridge Canyon Country 1994

Appendix B: MATLAB Code

B. 1 Parametric LQR for n-story building

```
clc; clear all
% T=3.5;
% wb=2*pi/T;
Ts=1.1758;
Ws=2*pi/Ts;  % for the main structure
stoheight=3;
beta0=0.05;
beta1=0.05;
beta2=0.05;
beta3=0.15;
beta4=0.20;
betaS=0.05;
%%%%%%%%%
epsi21=0.3;       %epsi21=w2/w1 % frequency ratio
%%%%%%%%%
n=12;              % Story number
ms=80;
alfa1=0.2;       %alfa1=m1/ms    % Mass ratio
b1=30;             % b is the assumed length and width of the structure which
is decided to be equal
b2=5;              % b2 length and width of the stiff core
%%%%%%%%%% MASS %%%%%%%%%%%%%%%%
MS1=ms*alfa1*eye(n);
MS2=ms*(1-alfa1)*eye(n);
Msteta1=ms*alfa1*b1^2/6*eye(n);
Msteta2=ms*(1-alfa1)*b2^2/6*eye(n);
M=[MS1 zeros(n,5*n);zeros(n,n) MS2 zeros(n,4*n);zeros(n,2*n) MS1
zeros(n,3*n);zeros(n,3*n) MS2 zeros(n,2*n);zeros(n,4*n) Msteta1 zeros(n,n);
zeros(n,5*n) Msteta2];
%%%%%%%%%%%% stiffness %%%%%%%
n1=n;
[ks]=kfinderff(ms,Ws,n);
[K1,K2]=k21fine(ms,ks,n1,epsi21,alfa1);
KI=(2*eye(n)+[zeros(n-1,1) -eye(n-1);zeros(1,n)]+[zeros(n-1,1) -eye(n-
1);zeros(1,n)]'-[zeros(n-1) zeros(n-1,1);zeros(1,n-1) 1]);
ks1=K1*KI;
ks2=K2*KI;
Kteta1=(K1*b1^2/4)*KI;
Kteta2=(K2*b2^2/4)*KI;
K=[ks1 zeros(n,5*n);zeros(n,n) ks2 zeros(n,4*n);zeros(n,2*n) ks1
zeros(n,3*n);zeros(n,3*n) ks2 zeros(n,2*n);zeros(n,4*n) Kteta1 zeros(n,n);
zeros(n,5*n) Kteta2];
%%%%%%%%%%%%%%%%%%%%%%%%%%%%%%%%%%%%%%%%%%%%%%%%%%%%
%%%%%%%%%%%%%% Periods
%Form the system matrix
A1=MS1\ks1;
[V1,D1]=eig(A1);
[D_sorted1, ind1] = sort(diag(D1),'ascend');
V_sorted1 = V1(:,ind1);
%Obtain natural frequencies and mode shapes
Wn11 = sqrt(D_sorted1(1));    Ts1=2*pi/Wn11;
Wn21 = sqrt(D_sorted1(2));
Wn31 = sqrt(D_sorted1(3));
mode11 = V_sorted1(:,1);
L11=(mode11'*MS1*ones(n1,1))/(mode11'*MS1*mode11);
[SA11]=specACmod11(Wn11,beta1);
dismod11=(L11*SA11/(Wn11^2))*mode11;
%%%%%%%%%%%%%%%%%%%   REIGHLEY    %%%%%%%%%%
```

```
a00n1=(2*beta1*Wn11*Wn31)/(Wn11+Wn31);
a11n1=(2*beta1)/(Wn11+Wn31);
Cs1=a00n1*MS1+a11n1*ks1;
%%%%%%%%%%%%%%%%%5second
A2=MS2\ks2;
[V2,D2]=eig(A2);
[D_sorted2, ind2] = sort(diag(D2),'ascend');
V_sorted2 = V2(:,ind2);
%Obtain natural frequencies and mode shapes
Wn12 = sqrt(D_sorted2(1));    Ts2=2*pi/Wn12;
Wn22 = sqrt(D_sorted2(2));
Wn32 = sqrt(D_sorted2(3));
mode12 = V_sorted2(:,1);
L22=(mode12'*MS2*ones(n1,1))/(mode12'*MS2*mode12);
[SA22]=specACmod12(Wn12,beta2);
dismod22=(L22*SA22/(Wn12^2))*mode12;
%%%%%%%%%%%%%%%%%%%   REIGHLEY    %%%%%%%%%%
a00n2=(2*beta2*Wn12*Wn32)/(Wn12+Wn32);
a11n2=(2*beta2)/(Wn12+Wn32);
Cs2=a00n2*MS2+a11n2*ks2;
%%%%%%%%%%%%%%%%%%%%%%%%%%%%%%%%%%%%%%%%%%%%%%%%
Cteta1=((Cs1(1)/2)*b1^2/4)*KI;
Cteta2=((Cs2(1)/2)*b2^2/4)*KI;
Cs=[Cs1 zeros(n,5*n);zeros(n,n) Cs2 zeros(n,4*n);zeros(n,2*n) Cs1
zeros(n,3*n);zeros(n,3*n) Cs2 zeros(n,2*n);zeros(n,4*n) Cteta1 zeros(n,n);
zeros(n,5*n) Cteta2];
%%%%%%%%%%%%%%%%%%%%viscous damp
md12=dismod11-dismod22;
cd=(4*pi*(ms*alfa1*sum(dismod11.^2)+ms*(1-
alfa1)*sum(dismod22.^2))*beta4)/(max(Ts1,Ts2)*sum(md12.^2));
CD1=cd*[eye(n1) -eye(n1);-eye(n1) eye(n1)];
CD=[CD1 zeros(2*n,4*n);zeros(2*n,2*n) CD1 zeros(2*n,2*n);zeros(2*n,6*n)];
C=Cs+CD;
% C=zeros(size(C));
% %%%%%%%%%%%%%%%%%%%%%%%%%%%%%%%%%%%    state
%%%%%%%%%%%%%%%%%%%%%%%%
A=[zeros(6*n) eye(6*n); -M\K -M\C ];
J11=[1 0 0 0 0 0
0 -1 0 0 0 0
0 0 1 0 0 0
0 0 0 -1 0 0
0 0 0 0 0 0
0 0 0 0 0 0];
J112=eye(n);
J=kron(J11,J112);
%for control force
B=[zeros(6*n) ; M\J];
%for seismic excitation as t5hese are two degree of freedom EQ
E=[zeros(6*n,1); -ones(4*n,1);zeros(2*n,1)];
% time of analysis
 % for the first sub structurre
TOPX1=cell(1,7);
TOPY1=cell(1,7);
TOPTETA1=cell(1,7);
TIMES=cell(1,7);
TOPX1MAX=zeros(1,7);
TOPY1MAX=zeros(1,7);
TOPTETA1MAX=zeros(1,7);
% for hw second structutre
TOPX2=cell(1,7);
TOPY2=cell(1,7);
TOPTETA2=cell(1,7);
TOPX2MAX=zeros(1,7);
TOPY2MAX=zeros(1,7);
TOPTETA2MAX=zeros(1,7);
```

```
% for the acceleration
% for the 1st structtutre
TOPACCELX1=cell(1,7);
TOPACCELY1=cell(1,7);
TOPACCELTETA1=cell(1,7);
TOPACCELX1MAX=zeros(1,7);
TOPACCELY1MAX=zeros(1,7);
TOPACCELTETAMAX=zeros(1,7);
INTDRIF=zeros(1,7);
% for the 2nd structure
TOPACCELX2=cell(1,7);
TOPACCELY2=cell(1,7);
TOPACCELTETA2=cell(1,7);
TOPACCELX2MAX=zeros(1,7);
TOPACCELY2MAX=zeros(1,7);
TOPACCELTETA2MAX=zeros(1,7);
INTDRIF2=zeros(1,7);

DT=[0.01, 0.005,0.005,0.02,0.005, 0.01, 0.01];
POINTS=[5590, 5437,6000, 2676,7277,4096,1999];
for rec=1:7
%load difinition
[TTT,TopX1,TopY1,TopTeta1,TopX1max,TopY1max,TopTeta1max,TopAccelX1,TopAccelY
1,TopAccelTeta1,TopAccelX1max,TopAccelY1max,TopAccelTeta1max,intdrif1,TopX2,
TopY2,TopTeta2,TopX2max,TopY2max,TopTeta2max,TopAccelX2,TopAccelY2,TopAccelT
eta2,TopAccelX2max,TopAccelY2max,TopAccelTeta2max,intdrif2]=calculatorLQR1(E
,n,A,B,M,K,rec,DT,stoheight);

TOPX1{rec}=TopX1;
arec='D:\EMU 2nd Semester courses\thesis\Matcode\all models\12 story
building\MR LQR\results\TOPX1rec';
brec=num2str(rec);
crec='.txt';
drec=[arec,brec,crec];
save(drec,'TopX1','-ascii');
TOPY1{rec}=TopY1;
arec='D:\EMU 2nd Semester courses\thesis\Matcode\all models\12 story
building\MR LQR\results\TOPY1rec';
brec=num2str(rec);
crec='.txt';
drec=[arec,brec,crec];
save(drec,'TopY1','-ascii');
TOPTETA1{rec}=TopTeta1;
arec='D:\EMU 2nd Semester courses\thesis\Matcode\all models\12 story
building\MR LQR\results\TopTeta1';
brec=num2str(rec);
crec='.txt';
drec=[arec,brec,crec];
save(drec,'TopTeta1','-ascii');
TOPX1MAX(1,rec)=TopX1max;
TOPY1MAX(1,rec)=TopY1max;
TOPTETA1MAX(1,rec)=TopTeta1max;
% for the 2nd structutre
TOPX2{rec}=TopX2;
arec='D:\EMU 2nd Semester courses\thesis\Matcode\all models\12 story
building\MR LQR\results\TOPX2rec';
brec=num2str(rec);
crec='.txt';
drec=[arec,brec,crec];
save(drec,'TopX2','-ascii');
TOPY2{rec}=TopY2;
arec='D:\EMU 2nd Semester courses\thesis\Matcode\all models\12 story
building\MR LQR\results\TOPY2rec';
brec=num2str(rec);
crec='.txt';
```

```
drec=[arec,brec,crec];
save(drec,'TopY2','-ascii');
TOPTETA2{rec}=TopTeta2;
arec='D:\EMU 2nd Semester courses\thesis\Matcode\all models\12 story
building\MR LQR\results\TopTeta2';
brec=num2str(rec);
crec='.txt';
drec=[arec,brec,crec];
save(drec,'TopTeta2','-ascii');
TOPX2MAX(1,rec)=TopX2max;
TOPY2MAX(1,rec)=TopY2max;
TOPTETA2MAX(1,rec)=TopTeta2max;
TOPACCELX1{rec}=TopAccelX1;
arec='D:\EMU 2nd Semester courses\thesis\Matcode\all models\12 story
building\MR LQR\results\TopAccelX1';
brec=num2str(rec);
crec='.txt';
drec=[arec,brec,crec];
save(drec,'TopAccelX1','-ascii');
TOPACCELY1{rec}=TopAccelY1;
arec='D:\EMU 2nd Semester courses\thesis\Matcode\all models\12 story
building\MR LQR\results\TopAccelY1';
brec=num2str(rec);
crec='.txt';
drec=[arec,brec,crec];
save(drec,'TopAccelY1','-ascii');
TOPACCELTETA1{rec}=TopAccelTeta1;
arec='D:\EMU 2nd Semester courses\thesis\Matcode\all models\12 story
building\MR LQR\results\TopAccelTeta1';
brec=num2str(rec);
crec='.txt';
drec=[arec,brec,crec];
save(drec,'TopAccelTeta1','-ascii');
TOPACCELX1MAX(1,rec)=TopAccelX1max;
TOPACCELY1MAX(1,rec)=TopAccelY1max;
TOPACCELTETAMAX(1,rec)=TopAccelTeta1max;
INTDRIF(1,rec)=intdrif1;
% for the 2nd structutre
TOPACCELX2{rec}=TopAccelX2;
arec='D:\EMU 2nd Semester courses\thesis\Matcode\all models\12 story
building\MR LQR\results\TopAccelX2';
brec=num2str(rec);
crec='.txt';
drec=[arec,brec,crec];
save(drec,'TopAccelX2','-ascii');
TOPACCELY2{rec}=TopAccelY2;
arec='D:\EMU 2nd Semester courses\thesis\Matcode\all models\12 story
building\MR LQR\results\TopAccelY2';
brec=num2str(rec);
crec='.txt';
drec=[arec,brec,crec];
save(drec,'TopAccelY2','-ascii');
TOPACCELTETA2{rec}=TopAccelTeta2;
arec='D:\EMU 2nd Semester courses\thesis\Matcode\all models\12 story
building\MR LQR\results\TopAccelTeta2';
brec=num2str(rec);
crec='.txt';
drec=[arec,brec,crec];
save(drec,'TopAccelTeta2','-ascii');
TOPACCELX2MAX(1,rec)=TopAccelX2max;
TOPACCELY2MAX(1,rec)=TopAccelY2max;
TOPTETA2MAX(1,rec)=TopAccelTeta2max;
INTDRIF2(1,rec)=intdrif2;
```

```
TIMES{rec}=TTT;
arec='D:\EMU 2nd Semester courses\thesis\Matcode\all models\12 story
building\MR LQR\results\TTT';
brec=num2str(rec);
crec='.txt';
drec=[arec,brec,crec];
save(drec,'TTT','-ascii');

end

save('D:\EMU 2nd Semester courses\thesis\Matcode\all models\12 story
building\MR LQR\results\TOPX1MAX.txt','TOPX1MAX','-ascii')
save('D:\EMU 2nd Semester courses\thesis\Matcode\all models\12 story
building\MR LQR\results\TOPY1MAX.txt','TOPY1MAX','-ascii')
save('D:\EMU 2nd Semester courses\thesis\Matcode\all models\12 story
building\MR LQR\results\TOPTETA1MAX.txt','TOPTETA1MAX','-ascii')

save('D:\EMU 2nd Semester courses\thesis\Matcode\all models\12 story
building\MR LQR\results\TOPX2MAX.txt','TOPX2MAX','-ascii')
save('D:\EMU 2nd Semester courses\thesis\Matcode\all models\12 story
building\MR LQR\results\TOPY2MAX.txt','TOPY2MAX','-ascii')
save('D:\EMU 2nd Semester courses\thesis\Matcode\all models\12 story
building\MR LQR\results\TOPTETA2MAX.txt','TOPTETA2MAX','-ascii')

save('D:\EMU 2nd Semester courses\thesis\Matcode\all models\12 story
building\MR LQR\results\TOPACCELX1MAX.txt','TOPACCELX1MAX','-ascii')
save('D:\EMU 2nd Semester courses\thesis\Matcode\all models\12 story
building\MR LQR\results\TOPACCELY1MAX.txt','TOPACCELY1MAX','-ascii')
save('D:\EMU 2nd Semester courses\thesis\Matcode\all models\12 story
building\MR LQR\results\TOPACCELTETAMAX.txt','TOPACCELTETAMAX','-ascii')
save('D:\EMU 2nd Semester courses\thesis\Matcode\all models\12 story
building\MR LQR\results\INTDRIF.txt','INTDRIF','-ascii')

save('D:\EMU 2nd Semester courses\thesis\Matcode\all models\12 story
building\MR LQR\results\TOPACCELX2MAX.txt','TOPACCELX2MAX','-ascii')
save('D:\EMU 2nd Semester courses\thesis\Matcode\all models\12 story
building\MR LQR\results\TOPACCELY2MAX.txt','TOPACCELY2MAX','-ascii')
save('D:\EMU 2nd Semester courses\thesis\Matcode\all models\12 story
building\MR LQR\results\TOPACCELTETA2MAX.txt','TOPACCELTETA2MAX','-ascii')
save('D:\EMU 2nd Semester courses\thesis\Matcode\all models\12 story
building\MR LQR\results\INTDRIF2.txt','INTDRIF2','-ascii')
```

B. 2 Parametric code for spectral acceleration

```
function [SA22]=specACmod12(Wn12,beta2)
Wn1=Wn12;
 Tt=2*pi/Wn1;
 BT=beta2;
Ss=1.415;        %MCER ground motion for 0.2 second period
S1= 0.494;        %MCER ground motion for 1.0 second period
Fa=1.2;         %Site amplification factor at 0.2 second
Fv=1.8;       %Site amplification factor at 1.0 second


Sms=Fa*Ss;               % Site-modified spectral acceleration value
Sm1=Fv*S1;               % Site-modified spectral acceleration value
Sds=(2/3)*Sms;           % Numeric seismic design value at 0.2 second SA
Sd1=(2/3)*Sm1;           % Numeric seismic design value at 1.0 second SA
T0=0.2*(Sd1/Sds);
Ts=Sd1/Sds;
Tl=6;                    % Long-period transition period in seconds



%%%%spectrum damping correction parameters
if BT<0.02
    dampa=0.8;
elseif 0.02<=BT && BT<0.05
    dampa=0.8+0.2*(BT-0.02)/0.03;
elseif 0.05<=BT && BT<0.1
    dampa=1+0.2*(BT-0.05)/0.05;

elseif 0.1<=BT && BT<0.2
    dampa=1.2+0.3*(BT-0.1)/0.1;

elseif 0.2<=BT && BT<0.3
    dampa=1.5+0.3*(BT-0.2)/0.1;

elseif 0.3<=BT && BT<0.4
    dampa=1.8+0.3*(BT-0.3)/0.1;

elseif 0.4<=BT && BT<0.5
    dampa=2.1+0.3*(BT-0.4)/0.1;

elseif 0.5<=BT && BT<0.6
    dampa=2.4+0.3*(BT-0.5)/0.1;

elseif 0.6<=BT && BT<0.7
    dampa=2.7+0.3*(BT-0.6)/0.1;

elseif 0.7<=BT && BT<0.8
    dampa=3+0.3*(BT-0.7)/0.1;

elseif 0.8<=BT && BT<0.9
    dampa=3.3+0.3*(BT-0.8)/0.1;

else
    dampa=3.6+0.4*(BT-0.9)/0.1;
end

T0=T0/dampa;

%%%%%%%%%%%%%%%

    if Tt<T0
        SA1=max(Sds*(0.4+0.6*Tt/(T0*dampa)),Sds*(1/dampa));
    end
    if T0<=Tt && Tt<=Ts
        SA1=Sds*(1/dampa);
```

```
    end
    if Ts<=Tt && Tt<=Tl
        SA1=(Sd1/Tt)*(1/dampa);
    end
    if Tl<Tt
        SA1=(1/dampa)*(Sd1*Tl)/(Tt^2);
    end
    SA22=SA1;
end
```

B. 2 Parametric code for stiffness calculation

```
function  [K1,K2]=k21fine(ms,ks,n1,epsi21,alfa1)
MS1=alfa1*ms*eye(n1);
MS2=(1-alfa1)*ms*eye(n1);
KI=(2*eye(n1)+[zeros(n1-1,1) -eye(n1-1);zeros(1,n1)]+[zeros(n1-1,1) -eye(n1-
1);zeros(1,n1)]'-[zeros(n1-1) zeros(n1-1,1);zeros(1,n1-1) 1]);
Wn1=1;
Wn2=10*epsi21;
K2=0;
while abs(((Wn2/Wn1)-epsi21)/epsi21)>0.01
K2=K2+0.000001*ks;
K1=ks-K2;
%%%%%
A1=MS1\(K1*KI);
[V1,D1]=eig(A1);
[D_sorted1, ind1] = sort(diag(D1),'ascend');
V_sorted1 = V1(:,ind1);
Wn1 = sqrt(D_sorted1(1));
%%%%%%%%%%
A2=MS2\(K2*KI);
[V2,D2]=eig(A2);
[D_sorted2, ind2] = sort(diag(D2),'ascend');
V_sorted2 = V2(:,ind2);
Wn2 = sqrt(D_sorted2(1));
end
end
```